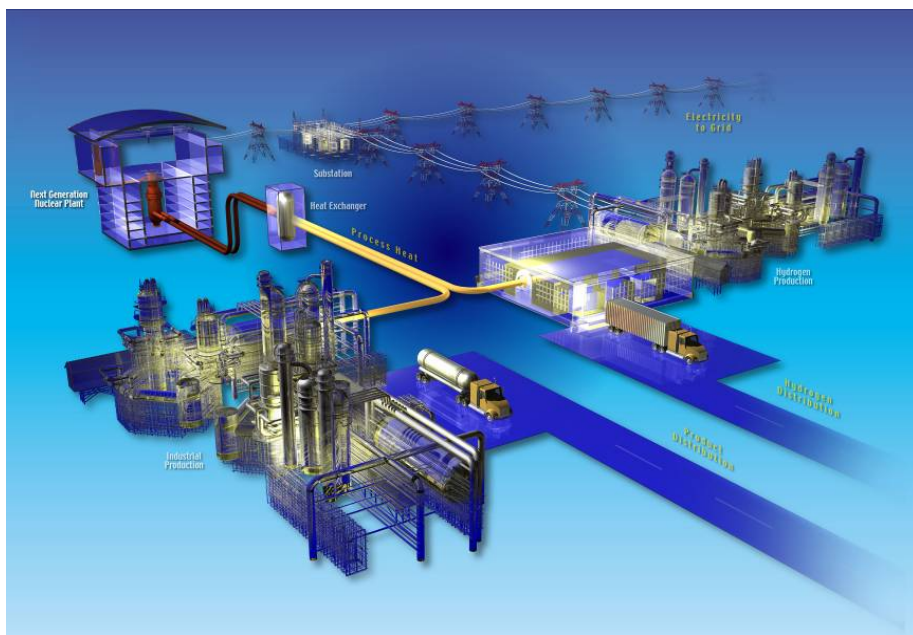


# FY 2008 Six-inch Diameter Coater Test Report

Charles M. Barnes  
Douglas W. Marshall

September 2008



#### **DISCLAIMER**

This information was prepared as an account of work sponsored by an agency of the U.S. Government. Neither the U.S. Government nor any agency thereof, nor any of their employees, makes any warranty, expressed or implied, or assumes any legal liability or responsibility for the accuracy, completeness, or usefulness, of any information, apparatus, product, or process disclosed, or represents that its use would not infringe privately owned rights. References herein to any specific commercial product, process, or service by trade name, trade mark, manufacturer, or otherwise, does not necessarily constitute or imply its endorsement, recommendation, or favoring by the U.S. Government or any agency thereof. The views and opinions of authors expressed herein do not necessarily state or reflect those of the U.S. Government or any agency thereof.

# **FY 2008 Six-inch Diameter Coater Test Report**

**Charles M. Barnes  
Douglas W. Marshall**

**September 2008**

**Idaho National Laboratory  
Next Generation Nuclear Plant Project  
Idaho Falls, Idaho 83415**

**Prepared for the  
U.S. Department of Energy  
Office of Nuclear Energy  
Under DOE Idaho Operations Office  
Contract DE-AC07-05ID14517**



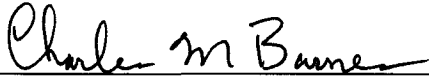
## Next Generation Nuclear Plant Project

# FY 2008 Six-inch Diameter Coater Test Report

INL/EXT-08-14633

September 2008


Approved by:

  
\_\_\_\_\_  
Charles M. Barnes, author

9/10/08  
\_\_\_\_\_  
Date

  
\_\_\_\_\_  
Douglas W. Marshall, author

9/10/08  
\_\_\_\_\_  
Date

  
\_\_\_\_\_  
John R. Cox  
Technology Development Office Deputy Director

9/10/08  
\_\_\_\_\_  
Date

  
\_\_\_\_\_  
David A. Petti  
Technology Development Office Director

9/10/08  
\_\_\_\_\_  
Date



## SUMMARY

As part of the Next Generation Nuclear Plant Project/Advanced Gas Reactor Fuel Development and Qualification Program, 30 tests were performed in a 6-inch diameter coater by Babcock and Wilcox (B&W) in FY 2008. These tests had three purposes: to determine coating conditions that would produce particles meeting AGR-2 fuel specifications, to provide data to select variant coating conditions for the silicon carbide (SiC) layer, and to obtain and evaluate pressure fluctuation data as a real-time indicator of coater fluid dynamics and an early indicator of particle properties.

Hot samples of buffer and inner pyrolytic carbon (IPyC) particles were taken during these tests to enable measurement of buffer and IPyC layer properties that cannot be measured on fully-coated particles. While the sampler proved adequate for these tests, modification of the design is recommended to enable taking both buffer and IPyC samples in a single coating run and to increase the quantity of particles obtained in the sample.

Early in the year, the methyltrichlorosilane (MTS) system was replaced with a modified design to enable better control of the MTS rate to the coater. While control of MTS improved with the modified system, it was found to be labor intensive, requiring constant monitoring of the MTS pot effluent rate, and at times, making adjustments of sweep gas, MTS pot temperature, or silicon carbide (SiC) coating time. Replacement of the current MTS system with a direct liquid injection system is recommended.

Surrogate kernels were used in seven tests, while natural uranium oxycarbide (NUCO) kernels were used in the remainder of the tests. These NUCO kernels were from three different kernel lots, and provided information of how small differences in kernel properties affect coating properties. A kernel charge size of 1.5 kg was used in 12 tests and of 1.3 kg in the remainder of the tests. Early results showed improvements in pyrocarbon anisotropy and particle aspect ratio with the smaller charge, but these benefits were not confirmed by later results. Future tests with increased kernel charges are planned to determine the maximum charge size that can be coated in the B&W coater without compromising particle quality.

Particles with buffer densities meeting the AGR-2 fuel specification were produced over a range of buffer coating conditions. However, in a series of runs that sought to use the same buffer coating conditions, buffer densities varied from the desired  $1.05 \text{ g/cm}^3$  to as low as  $0.94 \text{ g/cm}^3$ . To avoid the risk of not meeting the buffer density specification in future runs, tests are recommended to better determine the effect of process conditions on buffer density and to reduce its variability from run to run.

The density of the IPyC layer is determined primarily by coater temperature. It was found that the required bed temperature which resulted in an IPyC density of  $1.90 \text{ g/cm}^3$  in the B&W coater was nearly identical to the IPyC temperature used to achieve the same density for AGR-1 particles in the smaller Oak Ridge National Laboratory (ORNL) coater. At this coating temperature and a coating gas fraction (CGF) of 0.3, particles with acceptable IPyC anisotropy

and surface connected porosity were produced. Only two tests were performed with IPyC CGFs greater than 0.3, but the results from these tests and AGR-1 coating development tests suggest that IPyC CGFs of 0.35–0.40 may reduce the IPyC anisotropy and allow for the higher coating gas flows needed if the kernel charge size is increased.

SiC layer coating tests included runs with varying concentrations of MTS and argon. At a control temperature of 1600°C, it was found that the MTS concentration must be limited to less than 2 mol% for hydrogen-dilution only application of SiC. At higher MTS concentrations, the SiC average density would be less than the specified value of  $\geq 3.19 \text{ g/cm}^3$ . However, adding 20–30% argon to the fluidization gas allowed us to increase the concentration of MTS and reduce the coating temperature, while still achieving the desired layer density. The AGR-2 variant conditions for the SiC layer of UCO coated particles include a control temperature of 1550°C, estimated to correspond to a bed temperature of 1430–1450°C, and 30% argon. The maximum MTS concentration that could be used and a more precise optimum argon concentration were not determined. Higher MTS concentrations are favored by economics, as they result in higher coating rates and lower coating times, while thermodynamics limit the MTS concentration with argon dilution.

The specification for SiC microstructure was easily met for both baseline (hydrogen-only) and variant (hydrogen-argon dilution) cases. For both cases, a very fine grain microstructure was obtained, similar to German particles. This fine grain structure prevented using an optical examination of burned back particles to determine gold spots. Instead, particles were mounted and sectioned and the SiC layer was examined for circumferential defects or inclusions. Unlike AGR-1 particles, essentially no SiC inclusions were found in most of the batches of B&W particles examined.

Twenty-six batches of particles were examined for SiC defects by the burn-leach method, including particles from 22 tests plus four AGR-2 production runs. The number of defective particles found, in samples of 50,000 particles, ranged from  $<0.2$  to 67. The defect fraction correlated with SiC thickness but not with any SiC coating parameter. For particle batches with SiC thicknesses greater than or equal to  $34.5 \text{ }\mu\text{m}$ , one batch failed the SiC defect fraction specification compared to 11 batches that passed the defect specification. Changes in sieving and tabling methods appeared to increase the frequency of meeting the SiC defect fraction specification. However, the revised tabling practice results in widely varying particle yields, from approximately 50% to 90%. Additional characterization of reject particles and particle upgrading studies are recommended toward the objective of consistently obtaining high yields of particles.

Consistent with results for AGR-1 coating, the outer pyrocarbon (OPyC) layer was found to require a higher coating temperature than the IPyC layer to achieve the same layer density. It was also found that the change in density with temperature is greater for the OPyC layer than the IPyC layer. OPyC anisotropies for all tests were well within the specification limit and lower than IPyC anisotropies. In part this was due to the higher coating temperature of OPyC



coating and in part due to the high temperature the IPyC layer experiences during SiC coating.

Though coating conditions for the IPyC and OPyC layers were very similar, OPyC surface connected porosities, typically 0.4–0.8 ml/m<sup>2</sup>, were much lower than IPyC surface connected porosities, typically 2.0–2.4 ml/m<sup>2</sup>. The difference in porosities was in part due to the higher coating rate used for the IPyC layer. To achieve higher OPyC surface connected porosities, higher gas flows are needed during OPyC coating. In conjunction with studies to determine the maximum charge size, an evaluation of modifications needed to the off-gas system to allow for higher flow rates will be performed.

Samples from several OPyC batches of particles were measured for OPyC porosity by both B&W and ORNL with significantly different results. Though both laboratories use porosimeters manufactured by Quantachrome, the differences in the results appear to be due to differences in the instrument model used, with B&W having the latest model. Further analyses of particles and comparisons of porosimetry data are recommended to resolve these differences, including upgrading the ORNL porosimeter.

During all coating tests, pressure fluctuations and total system back pressure were monitored in order to understand the impact of process changes on bed hydrodynamics and to determine if these pressure data could be correlated with particle properties. Possible correlations have been found between reduced pressure transducer data and particle properties. The most encouraging correlation is with pyrocarbon anisotropy. A strong correlation was also found between pressure parameters and particle aspect ratio.

Six coating runs, four using baseline conditions and two using variant conditions, were made with low enriched uranium kernels to produce particles that can be used for AGR-2 fuel. Final selection of the particular batches that will be compacting for AGR-2 UCO fuel will be made once the particles from these runs are fully characterized.



# CONTENTS

SUMMARY .....	vi
ACRONYMS .....	xiv
1. INTRODUCTION .....	1
2. KERNEL PROPERTIES .....	2
3. BUFFER LAYER .....	3
4. IPyC LAYER .....	5
4.1 IPyC Density .....	5
4.2 IPyC Anisotropy .....	6
4.3 IPyC Surface Connected Porosity and IPyC-SiC Interface .....	8
5. SiC LAYER .....	10
5.1 SiC Density .....	10
5.2 SiC Defects .....	11
5.3 SiC Microstructure .....	12
5.4 SiC Inclusions .....	14
5.5 SiC and OPyC Aspect Ratio .....	16
5.6 Selection of Variant SiC Conditions .....	16
6. OUTER PYROLYTIC CARBON LAYER .....	18
6.1 OPyC Density .....	18
6.2 OPyC Anisotropy .....	19
6.3 Missing OPyC Layers .....	21
6.4 OPyC Surface Connected Porosity .....	21
7. PRESSURE FLUCTUATION DATA ANALYSIS .....	24
8. TABLING YIELD AND KERNEL CHARGE SIZE .....	33
9. COATING AGR-2 UCO PARTICLES .....	34
10. CONCLUSIONS, RECOMMENDATIONS AND PLANS .....	35
11. REFERENCES .....	37
Appendix A Coater Run Data .....	39

## FIGURES

Figure 1. Buffer density versus control temperature, coating gas fraction and coating rate.....	4
Figure 2. IPyC density versus bed temperature. ....	6
Figure 3. IPyC anisotropy versus coating rate, coating gas fraction, and temperature for the 2-inch coater. ....	7
Figure 4. IPyC anisotropy versus bed temperature, 6-inch-diameter coater. ....	7
Figure 5. IPyC diattenuation versus average coating rate and coating gas fraction.....	8
Figure 6. IPyC surface connected porosity versus coating rate and coating gas fraction. ....	9
Figure 7. Examples of IPyC/SiC interface (from batch 93056).....	9
Figure 8. SiC density versus MTS concentration and other coating parameters. ....	11
Figure 9. SiC defects versus layer thickness.....	12
Figure 10. Visual standard for SiC microstructure showing particle with too large a grain size.....	13
Figure 11. Comparison of SiC microstructure. ....	13
Figure 12. The one SiC inclusion found in sample of 93060 particles. ....	15
Figure 13. SiC and OPyC aspect ratios.....	16
Figure 14. SiC phase boundaries and target operating points.....	17
Figure 15. Comparison of pyrocarbon density versus bed temperature data. ....	18
Figure 16. Pyrocarbon density versus temperature for B&W coater. ....	19
Figure 17. Pyrocarbon equivalent anisotropies verses bed temperature for B&W 6-inch coater. ....	19
Figure 18. Pyrocarbon anisotropy versus coating rate. ....	20
Figure 19. Relationship of OPyC anisotropy to pressure drop across coater.....	21
Figure 20. Surface connected porosity versus average coating rate. ....	22
Figure 21. Plots of pressure fluctuations during the course of buffer deposition. ....	24
Figure 22. STFT plots of pressure fluctuations during the course of buffer deposition. ....	25
Figure 23. Plots of pressure fluctuations during the course of IPyC deposition. ....	26
Figure 24. Interpretation of features on a pressure fluctuation plot. ....	26
Figure 25. Rescaled range analysis (Pox) plot used for determining Hurst exponents.....	27
Figure 26. Representative Strange attractor plots for buffer deposition. ....	28
Figure 27. Autocorrelation plot showing features corresponding to maximum and minimum mutual information on Strange attractor plots. ....	28
Figure 28. Comparison of IPyC diattenuation measurements with predicted values. ....	29
Figure 29. Comparison of OPyC diattenuation measurements with predicted values.....	30
Figure 30. Illustration of apparent differences in the fluid dynamics for coated NUCO and zirconia surrogates. ....	31
Figure 31. Comparison of predicted to measured OPyC aspect ratios.....	32

## TABLES

Table 1. Properties of kernels used in FY 2008 coater tests. ....	2
Table 2. Buffer layer coating conditions and properties. ....	3
Table 3. Acceptance criteria for Stages 1, 2, and 3. ....	11
Table 4. Effect of cooling and upgrading on OPyC porosities. ....	22
Table 5. Comparison of ORNL and B&W porosity measurements. ....	23



## ACRONYMS

AGR	Advanced Gas Reactor
AGR-1	First irradiation test of the AGR program; lab-scale fabrication
AGR-2	Second irradiation test of the AGR program; (small) industrial-scale fabrication
B	a low density carbon (“buffer”) coating layer
BAF <sub>o</sub>	Bacon anisotropy factor
B&W	Babcock and Wilcox, formerly BWX Technologies (BWXT)
CGF	coating gas fraction
FY	fiscal year
INL	Idaho National Laboratory
JAERI	Japan Atomic Energy Research Institute
IPyC	inner pyrolytic carbon coating layer
LEU	low-enriched uranium
MTS	methyltrichlorosilane
NA	not applicable
NGNP	Next Generation Nuclear Plant
NUCO	natural uranium oxycarbide
OPyC	outer pyrolytic carbon (coating layer)
ORNL	Oak Ridge National Laboratory
SiC	silicon carbon (coating layer)
slpm	standard liters per minute
STFT	short-time Fourier transform
TC	thermocouple
TRISO	tristructural-isotropic (multilayer, isotropic coatings consisting of buffer, IPyC, SiC and OPyC layers)
UCO	uranium oxycarbide (may contain various fractions of uranium carbide (UC <sub>1.86</sub> ), uranium oxide (UO <sub>2</sub> ) and UC <sub>1-x</sub> O <sub>x</sub> )
YSZ	yttrium stabilized zirconia (microspheres used as surrogate UCO kernels)





# FY 2008 Six-inch Diameter Coater Test Report

## 1. INTRODUCTION

A production-scale coater must be demonstrated as part of the plan to develop and qualify fuel for the Advanced Gas Reactor (AGR).<sup>1</sup> A 2-inch-diameter coater was used to produce tristructural-isotropic (TRISO) coated particles for the first AGR experiment (AGR-1). An existing 6-inch-diameter coater was chosen to demonstrate industrial scale coating for the AGR-2 experiment.<sup>2</sup> A separate study<sup>3</sup> evaluated coater crucible and gas distributor designs and recommended the initial designs, which are now tested.

Following modifications to the coating process<sup>4</sup> at Babcock and Wilcox (B&W) facilities, coater tests were performed using 400- $\mu\text{m}$  yttria stabilized zirconia (YSZ) surrogate kernels followed by 520- $\mu\text{m}$  YSZ kernels. The 520- $\mu\text{m}$  surrogate kernel was used so that, after applying a buffer layer of about 50  $\mu\text{m}$ , hydrodynamic similarity to uranium oxycarbide (UCO) kernels would be achieved for the final three coating layers. One of the recommendations based on results from previously reported tests performed in FY 2007<sup>5</sup> was to replace the MTS (methyltrichlorosilane) vaporizer to achieve better control of the MTS rate and silicon carbide (SiC) thickness. In late 2007, three additional coating tests were made using 520- $\mu\text{m}$  surrogate kernels prior to replacement of the MTS vaporizer, followed by 27 tests after replacement. The first seven of these tests continued to use surrogate kernels; the next 22 used natural uranium oxycarbide (NUCO) kernels; 11 of which were performed prior to qualification runs followed by six qualification runs for baseline conditions and five qualification runs for variant conditions. The final test run used low-enriched uranium (LEU) UCO kernels. This report documents the results of these tests. Some results of earlier tests with the B&W coater and also some earlier data for the smaller Oak Ridge National Laboratory (ORNL) coater used for producing AGR-1 particles are included to more fully document how layer properties vary with coating conditions and how the coater scale affects these relationships.

The coater tests performed in FY 2008 had three purposes. The first purpose was to determine coating conditions that produce particles meeting the AGR-2 fuel specification.<sup>6</sup> The second was to provide data for selecting variant SiC coating conditions for AGR-2 fuel. Substituting argon for a portion of hydrogen during SiC coating has been reported in coating literature to offer advantages of less severe coating conditions without compromising SiC layer properties.<sup>7</sup> The third purpose was to obtain and evaluate pressure fluctuation data as a real-time indicator of coater fluid dynamics and determine if pressure data could be correlated with particle properties.

Section 2 of this report documents the properties of kernels used in the coating tests. Sections 3–6 describe test conditions and results for each of the four TRISO coatings, including comparisons of results for the tests at B&W with results of the smaller ORNL coater used for producing AGR-1 particles.

While it was not the intent of these tests to systematically determine relationships between coating parameters and their respective layer properties, comparing the B&W results with AGR-1 coater data provides some insight into the important ranges for coater parameters and their dependence on coater scale. The organization of test results by coating layer also permits easy comparison of layer properties with specifications. Section 6 documents results for the outer pyrolytic carbon (OPyC) layer and includes a comparison to the inner pyrolytic carbon (IPyC) layer because these two pyrocarbon layers are deposited using very similar conditions. Section 7 contains the evaluation of pressure fluctuation data. Even though the tests performed in FY 2008 were sufficient to qualify the coating process to produce AGR-2 particles, the results raised questions that should be answered before producing particles for AGR-5 and 6. Section 8 provides a brief discussion of kernel batch size and product yield, two areas that need further improvement for the coating process to be economic at full scale. Section 9 presents an outline of AGR-2 UCO coating runs. Section 10 provides recommendations and plans for additional tests

to prepare for coating particles for future AGR tests. Data from all coater tests performed in FY 2008 are included in Appendix A.

## 2. KERNEL PROPERTIES

Surrogate zirconia kernels plus UCO kernels from four separate composites were used in 2008 coater tests. Properties of these kernels are shown in Table 1. In tests using 520- $\mu\text{m}$  (nominal) YSZ kernels, a thin ( $\sim 50\text{ }\mu\text{m}$ ) buffer layer was applied so that the particle diameter and density for subsequent layers would be equivalent to UCO particles. Lot 69304 was a 20 kg lot of kernels produced in 2004 for these coater tests. Lot 69305 kernels were produced in kernel fabrication development tests prior to the campaign to produce 69304 kernels. Kernel fabrication conditions were deliberately varied in these tests and hence the kernels were not as consistent in properties as later kernel production runs, still, all properties met specifications. Lot 69306 kernels were produced in early 2008, using natural uranium. Kernel batch 59374 was produced during the campaign to produce AGR-2 kernels using enriched uranium, but was not included in the AGR-2 kernel lot (69307) because ceramographic images showed a small fraction of kernels with lenticular voids. This batch of approximately 1075 g of kernels were supplemented with 225 g of kernels from the AGR-2 kernel composite to make up the charge for coater run 93070.

Table 1. Properties of kernels used in FY 2008 coater tests.

Property	Kernel Lot (coating runs)				
	YSZ Surrogate (93033-35 & 93044-47)	69304 (93048–93060)	69305 (93061–93065)	69306 (93066–93069)	59374/ 69307 (93070)
Mean diameter, microns	516 <sup>a</sup>	429.0	432.1	420.7	426.5
Diameter standard deviation	31	8.9	12.2	7.1	NA
Mean aspect ratio	Not measured	1.005	1.018	1.010	1.016
Mean density, g/cm <sup>3</sup>	6.0	10.71	10.88	10.97	10.96
Density standard deviation	Not measured	0.01	0.21	0.04	NA
C/U atomic ratio	NA	0.37	0.39	0.39	0.39
O/U atomic ratio	NA	1.48	1.45	1.47	1.42
Total uranium, wt %	NA	89.1	89.5	89.3	89.6
U-235 enrichment, wt%	NA	natural	natural	natural	14.0

a. Based on B&W Camsizer measurement of >157,000 kernels. Mean diameter based on vendor analysis of 101 kernels is 528 microns.

### 3. BUFFER LAYER

The primary purpose of the buffer layer is to provide void volume for accumulating fission gases and CO produced in the kernel during irradiation. The buffer layer also absorbs the kinetic energy from recoiling fission fragments, thereby reducing damage to the IPyC layer. Thus a low density ( $1.05 \pm 0.10 \text{ g/cm}^3$ ) is specified for the buffer layer as well as minimum and mean layer thickness. The most important coating parameter in determining buffer density is the coating gas fraction, or equivalently, the hydrocarbon partial pressure in the coater.<sup>7, 8, 9</sup> Bed temperature, kernel charge size and acetylene flow rate can also affect the buffer density. Once conditions are established that achieve the specified coating density, the desired layer thickness can be obtained by adjusting the coating time.

For all runs made in FY 2008, the control temperature for buffer coating was set at 1470°C. Based on the internal thermocouple (TC) measurements for runs 93033 through 93047, the bed temperature at the beginning of buffer coating was about 1390°C and increased to about 1540°C degrees by the end of the short (4–7 minutes) coating. In contrast, with a small coater, such as the one used for AGR-1 particles, the buffer coating temperature can be controlled at a constant value. For AGR-1 particles, the buffer coating bed temperature was a constant 1450°C, resulting in buffer layer densities of 1.08–1.11 g/cm<sup>3</sup>.

There is currently no method available to determine buffer density from a fully coated particle so a “hot sample” of buffer coated particles is taken during the coating run. Hot samples were taken during nine of the tests made in 2008, plus two runs coating LEU kernels for AGR-2. Conditions and results of these runs for the buffer layer are shown in Table 2.

Table 2. Buffer layer coating conditions and properties.

Run #	Kernel charge	Control Temp (°C)	C <sub>2</sub> H <sub>2</sub> flow (slpm)	Primary argon flow (slpm)	Annulus argon flow (slpm)	Total gas flow (slpm)	Coating time (min)	Coating gas fraction	Layer thickness (μm)	Density, (g/cm <sup>3</sup> )	Coating rate (μm/min)
93048	1.50 kg NUCO	1473*	88	49	26	163	6.7	0.54	106.1	1.10	15.8
93054	1.30 kg NUCO	1473	92.8	43.5	18.9	155.2	5.4	0.60	118	1.09	21.9
93055	1.30 kg NUCO	1474	97.6	39	26	162.6	5.2	0.60	112.1	1.05	21.6
93057	1.30 kg NUCO	1473	93.1	43.6	18.9	155.6	4.6	0.60	102.7	1.07	22.3
93061	1.30 kg NUCO	1474	97.4	39	26	162.4	4.1	0.60	94.9	1.03	24.1
93062	1.30 kg NUCO	1474	97.5	39	26	162.5	4.1	0.60	97.2	0.94	23.2
93064	1.30 kg NUCO	1473	97.5	39	26	162.5	4.1	0.60	100	0.96	24.4
93066	1.30 kg NUCO	1474	97.5	39.1	26.1	162.7	4.25	0.60	101.5	0.96	23.9
93068	1.31 kg NUCO	1474	97.4	39	26.1	162.5	4.25	0.60	92.6	0.94	21.8
93072	1.3 kg LEU UCO	1474	99.5	39	25.9	164.4	4.25	0.61	95.0	1.04	22.4
93074	1.3 kg LEU UCO	1474	99.4	39	25.8	164.2	4.25	0.61	95.6	1.04	22.5

\* Temperature in doubt due to thermocouple (TC) drift; estimated temperature is 1510°C

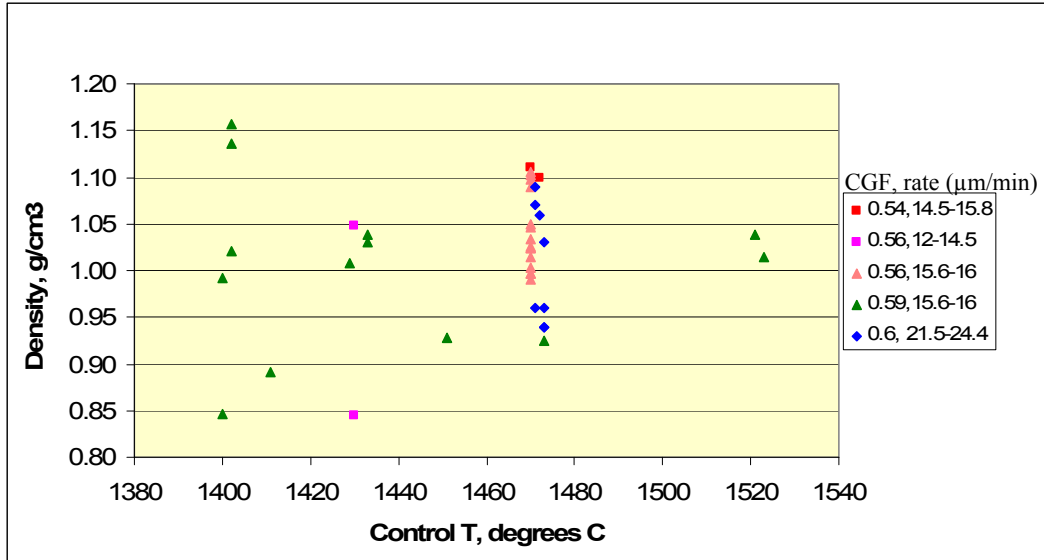


Figure 1. Buffer density versus control temperature, coating gas fraction and coating rate.

A better understanding of how buffer density varies with coating parameters is needed in order to ensure that densities can be controlled to within specification limits for future production runs. A study is recommended in which buffer temperature and gas flow rate are systematically varied, keeping kernel charge and other parameters constant. If changes in these two variables do not significantly affect buffer density, other coating gas fractions should also be tested.

Also, because a range of densities was observed in different runs in which no parameter was intentionally changed, further analysis of data from these tests or future runs is warranted to determine the causes of this variability.

## 4. IPyC LAYER

The purposes of the IPyC layer include providing an impermeable barrier to prevent chlorine-containing gases from reaching and reacting with the kernel during SiC coating, delaying transport of fission products from the kernel to the SiC layer, and providing the first structural layer to contain fission product gases. When tightly bonded to the SiC layer, shrinkage of the IPyC layer during irradiation helps to maintain the SiC layer in compression. IPyC specifications include the mean layer thicknesses, upper and lower critical limit layer thicknesses, a mean anisotropy limit, and an anisotropy upper critical limit. Another IPyC property of interest is the surface connected porosity, as this is an indication of the ability of SiC to infiltrate and bond with the IPyC layer.

While coating AGR-1 particles, a systematic study was conducted in the ORNL 2-inch-diameter coater to determine how IPyC properties varied as coater temperature and coating gas fraction were varied.<sup>10</sup> These relationships provided a guide for tests in the 6-inch coater. Results from these small coater tests showed:

- IPyC density is primarily dependent on coater temperature and less dependent on coating gas fraction and total gas flow.
- Anisotropy is primarily dependent on coating rate, which in turn is affected by coating temperature, coating gas fraction, coating gas flow rate, and coater batch size.
- Surface connected porosity is primarily dependent on coating gas fraction and secondarily on coating temperature.

### 4.1 IPyC Density

A comparison of the relationship between IPyC density and bed temperature for both the ORNL and B&W coaters is charted in Figure 2. The trend lines show that, at a temperature of about 1265°C, both coaters result in IPyC layers at the specified mean density of 1.90 g/cm<sup>3</sup>. The change in density with temperature is less for the larger coater than the smaller coater. This will allow a wider operating region for the 6-inch-diameter coater to produce particles with the specified density. Most of the data shown on Figure 1 are from tests performed in 2007 as the internal thermocouple was removed from the B&W coater in early 2008.

Hot samples of IPyC-coated particles were taken in 19 test runs plus two AGR-2 particle runs. In the first series of five runs, coating gas fraction, IPyC flow rates and coater charge size were varied, keeping coating temperature constant. IPyC densities for these runs were in the narrow range of 1.874–1.905 g/cm<sup>3</sup>, confirming that the variations in coating conditions had little effect on layer density. In the next series of six runs, all IPyC conditions were held constant. These runs were performed in sequence without obtaining characterization data from any run before completing the series. When pyrocarbon densities data became available, it was apparent that the control TC had drifted as densities for both pyrocarbon layers departed from the expected and mean specification value of 1.90 g/cm<sup>3</sup> and were within the range of 1.78–1.86 g/cm<sup>3</sup>. After replacing the TC, and using the same IPyC conditions that were used for the previous series, an IPyC density of 1.854 g/cm<sup>3</sup> was measured for the first run, followed by densities of 1.913, 1.898, and 1.893 g/cm<sup>3</sup> for subsequent runs. Due to a break in a companion TC at that point, the control TC was replaced again, and very consistent IPyC densities were obtained for the final six runs, in the narrow range of 1.884–1.902 g/cm<sup>3</sup>.

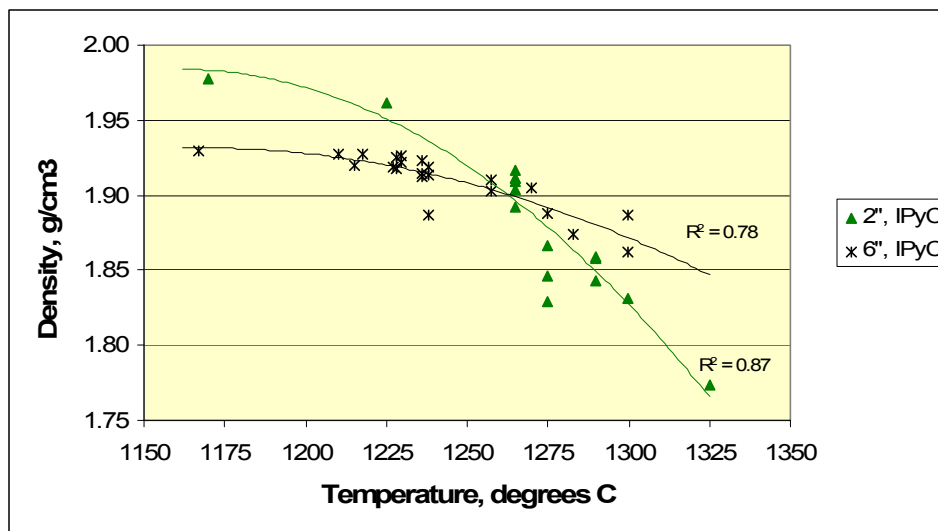


Figure 2. IPyC density versus bed temperature.

While these results show that specification IPyC densities can be repeatably achieved, the drift seen in the control TC in one series of tests and the spread in density data indicate the need to consider obtaining more accurate and consistent temperature control. If this is not possible, modifications to procedures or instrumentation should be considered to obtain early warning of TC drift. Power output to the furnace was reviewed subsequent to each AGR-2 coating run as a means to identify TC drift.

## 4.2 IPyC Anisotropy

Figure 3 shows the relationship between IPyC anisotropy and coating temperature, coating gas fraction, and average coating rate for the AGR-1 coater. At constant coating gas fraction, anisotropy decreases as the coating temperature increases. As the coating gas fraction increases, the rate of decrease with increasing temperature decreases. For a given temperature in the range 1225–1275°C, there is a coating rate that gives a minimum anisotropy. And while the coating rate at which the minimum anisotropy occurs increases with coating temperature, the coating gas fraction at which it occurs appears to be fairly constant at approximately 0.32–0.35. These results, assuming they apply to the larger coater, would suggest increasing the IPyC coating gas fraction specification (currently  $0.3 \pm 0.03$ ) to a slightly higher value or a wider range. Figure 3 shows trend lines connecting data for constant coating gas fractions. While the trend for data points from runs using a coating gas fraction of 0.15 is nearly linear, the data for the other two coating gas fractions suggest a more complex relationship that decreases in slope at higher coating rates.

IPyC anisotropies for runs made in B&W's coater were found to generally follow the same trends as shown in Figure 3. Anisotropy decreases with increasing temperature (Figure 4) and increasing coating rate (Figure 5). Bed temperatures shown on Figure 4 for many of the tests were estimated based on IPyC densities as no direct measurement of bed temperatures were taken during these runs. These estimates, as well as uncertainties in the measured bed temperatures for runs when the internal TC was present, may account for some of the scatter in the data seen in Figure 4. Variations in coating rate also account for some of the scatter seen on Figure 4. Pyrocarbon anisotropy was measured for two separate samples of 93046 particles, and while these points appear abnormally low on Figure 4, the IPyC coating rate for this run was  $4.17 \mu\text{m}/\text{min}$  compared with about  $3.5 \mu\text{m}/\text{min}$  for other runs at the same temperature. The cause for the higher coating rate for run 93046 has not been discovered.

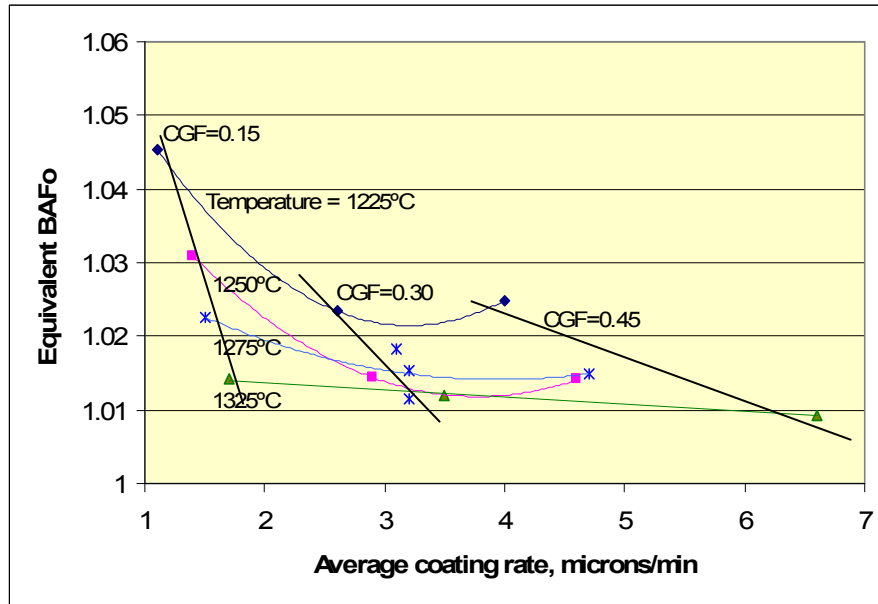


Figure 3. IPyC anisotropy versus coating rate, coating gas fraction, and temperature for the 2-inch coater.

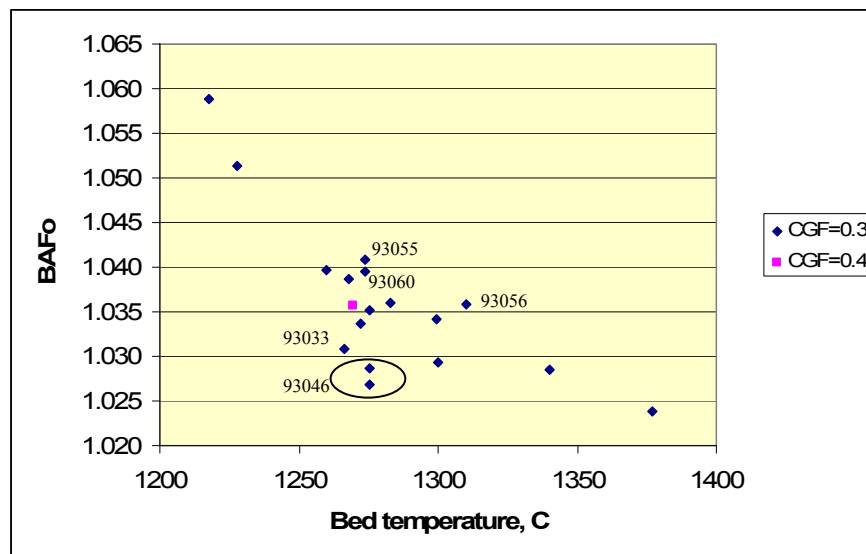


Figure 4. IPyC anisotropy versus bed temperature, 6-inch-diameter coater.

Figure 5 shows data for both the 2-inch ORNL and 6-inch B&W coaters. For a coating gas fraction of 0.3, the diattenuation of the IPyC layer of particles produced in the 6-inch coater are about 0.01 greater than those produced in the smaller coater at a similar coating rate. Scatter in the data shown on Figure 5 likely represents effects of temperature.

The effect of gas flow rate on IPyC anisotropy was not fully explored. One test was made in which the total gas flow rate was increased by about 14%, and no significant change was seen in the IPyC anisotropy. Likewise, the one test using a coating gas fraction of 0.4 was insufficient to determine the optimum coating gas fraction. Additional tests using IPyC coating gas fractions of 0.35–0.4 are recommended.

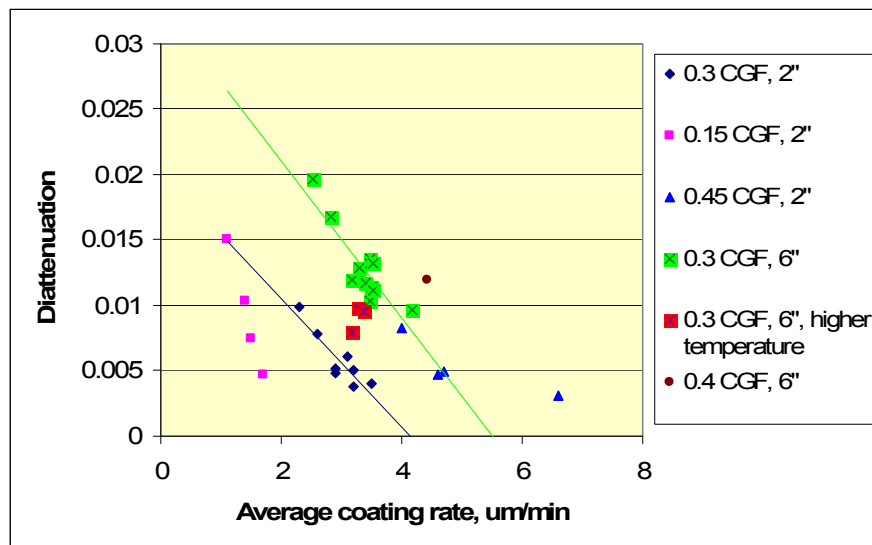


Figure 5. IPyC diattenuation versus average coating rate and coating gas fraction.

The AGR-2 specification for the mean IPyC anisotropy is  $\leq 1.045$  (diattenuation  $\leq 0.015$ ). Based on data for a coating gas fraction of 0.3, this can be achieved at bed temperatures greater than 1250°C and coating rates greater than about 3.2  $\mu\text{m}/\text{min}$ , as shown in Figures 4 and 5. The IPyC anisotropy specification thus sets a lower limit for the IPyC coating temperature while the IPyC density specification sets the upper limit.

### 4.3 IPyC Surface Connected Porosity and IPyC-SiC Interface

Surface connected porosity increases with increasing coating temperature, coating gas fraction, and coating rate. Figure 6 shows IPyC surface connected porosities measured with a mercury porosimeter over the pressure range 250–10,000 psi for both the ORNL 2-inch and B&W 6-inch diameter coaters. The ORNL data shows the trends of increasing porosity with increasing coating gas fraction and coating rate. For a coating gas fraction of 0.3, data for the B&W coater is very comparable to that for the ORNL coater. The B&W coater will result in particles with a higher IPyC surface connected porosity than was measured for AGR-1 particles because the IPyC coating rate is higher. However, the one data point from a B&W test using a coating gas fraction of 0.4 did not show a higher surface connected porosity than particles from tests at coating gas fractions of 0.3.

Even though no porosity specifications are imposed on the coated particles, a minimum porosity of 1.3  $\text{ml}/\text{m}^2$  is desired to ensure sufficient SiC infiltration into the IPyC layer, which in turn produces a strong IPyC/SiC bond. Figure 6 shows that coating rates greater than about 3  $\mu\text{m}/\text{min}$  will produce particles with porosities above the target minimum. Thus, the conditions that are needed for achieving the specified IPyC anisotropy will result in acceptable surface connected porosity.

An example of the IPyC/SiC interface typical of B&W particles is shown in Figure 7.



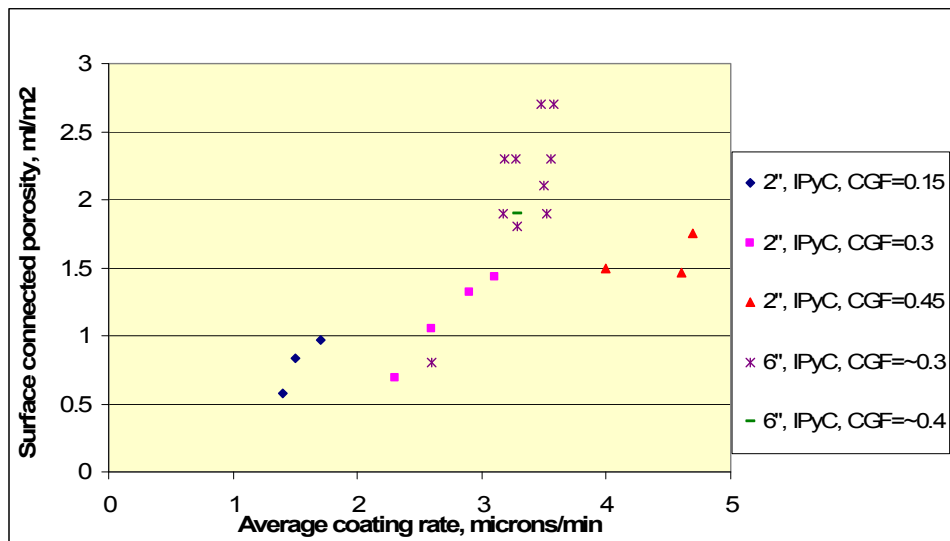


Figure 6. IPyC surface connected porosity versus coating rate and coating gas fraction.

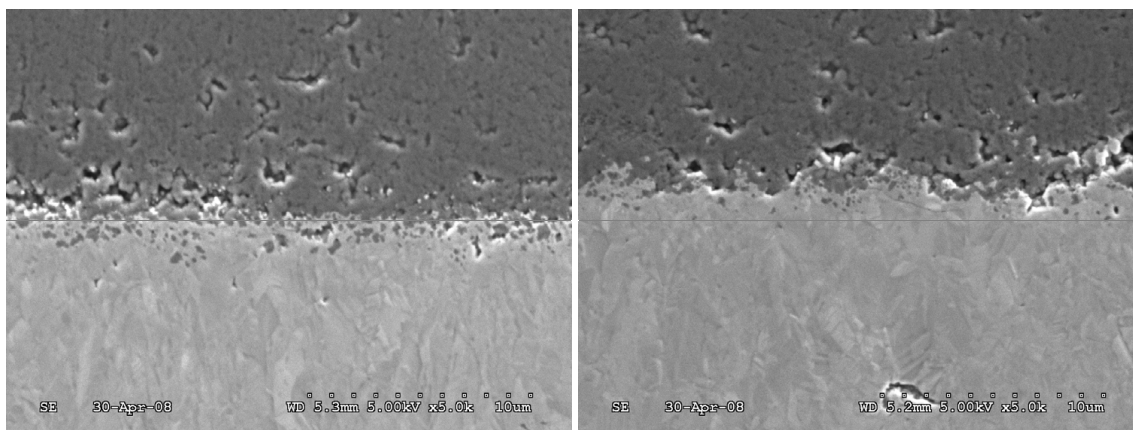


Figure 7. Examples of IPyC/SiC interface (from batch 93056).

## 5. SiC LAYER

The SiC layer provides the primary structural support that contains internal gas pressure generated during irradiation. It also prevents release of fission gases and metallic fission products. To ensure that these functions are accomplished, requirements are imposed for the layer thickness, density, microstructure, defect fraction, and the SiC-coated particle aspect ratio. For information only, particles are examined for a second type of defect fraction, formerly known as “gold spots,” but more accurately being circumferential delaminations or soot inclusions within the SiC layer.

Silicon carbide is deposited by decomposition of MTS at temperatures typically in the range 1450–1550°C. At lower temperatures, the deposit may contain free silicon and have a lower density than desired. At higher temperatures, the grain size is too large, allowing excessive diffusion of fission products.

To avoid free carbon in the deposit, a relatively high ratio of hydrogen to MTS (greater than about 30) is needed.<sup>11</sup> At these high hydrogen and low MTS concentrations, coating rates are typically less than 0.3  $\mu\text{m}/\text{min}$ , making the coating time for a 35- $\mu\text{m}$  layer on the order of 2 hours—much longer than the other layers. Partial replacement of the hydrogen diluent with argon has been reported to achieve desired layer properties at lower temperatures,<sup>7</sup> and was used to produce one of the AGR-1 variants.<sup>12</sup> As discussed in Section 5.6, a set of conditions that included partial argon dilution for SiC deposition was also determined for an AGR-2 UCO variant.

### 5.1 SiC Density

Figure 8 shows the relationship between SiC density, MTS concentration, argon concentration, and temperature. The dark blue data points are from runs that used hydrogen only for fluidization and dilution. The control temperature for all these runs was 1600°C, corresponding to bed temperatures of 1430–1500°C. Even though the control temperature set point remained constant for these 18 runs, bed temperature may have varied due to differences in kernel type, kernel charge size and small variations in the control thermocouple position and calibration.

In spite of these differences, SiC density clearly decreases with increasing MTS concentration for hydrogen-only diluent runs. At this temperature, to reliably achieve a SiC density greater than 3.19  $\text{g}/\text{cm}^3$ , the MTS concentration needs to be limited to less than 2.0%. This limit is identical to the current AGR-2 coating process specification limit.

Higher SiC densities can be obtained at higher MTS concentrations using argon dilution. Near theoretical SiC density was achieved in a test using 20% argon, 3% MTS, and a control temperature of 1600°C. Densities comfortably above the specification limit of 3.19  $\text{g}/\text{cm}^3$  were achieved in eight tests with a control temperature of 1550°C and MTS concentrations of 2.78–3.17%. In one of these eight tests, the argon concentration was 20%, while it was 30% in the other seven tests. One final test at a control temperature of about 1400°C resulted in a SiC density of 3.145  $\text{g}/\text{cm}^3$ . No internal thermocouple was present in any of the tests that used argon codilution, so the bed temperature for these runs is not known.

Coating times of the 30% argon variant runs with about 3 vol% MTS were reduced by only about 10% relative to the baseline SiC conditions. This was because total gas flows were reduced about 36% to maintain similar fluidizing conditions. The coating rate could be increased further by increasing total gas flows, which would in turn allow further reductions in SiC coating time.

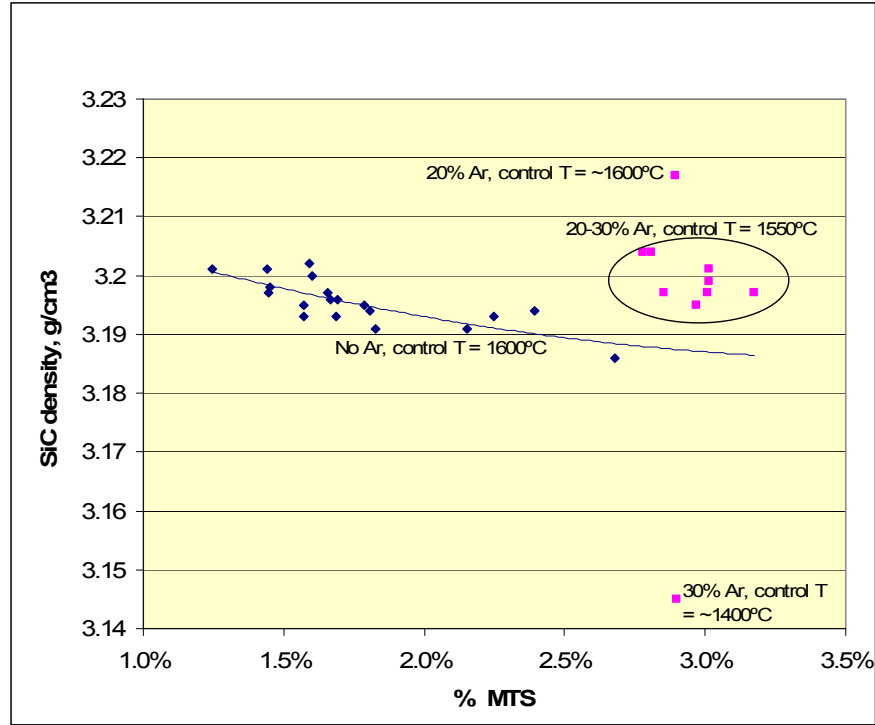


Figure 8. SiC density versus MTS concentration and other coating parameters.

## 5.2 SiC Defects

The SiC defect fraction is likely the single most important measure of particle quality, yet the coater design and operating conditions that affect this property have not been clearly identified. SiC defects were measured for samples from 22 test runs plus four coating runs of AGR-2 particles. Defects varied by over two orders of magnitude in these samples, from a low of  $<0.2$  defects to a high of 67 defects, for samples of 50,000 particles. The specification limit of  $1 \times 10^{-4}$  corresponds to the acceptance criteria in Table 3.

Table 3. Acceptance criteria for Stages 1, 2, and 3.

	Sample Size	Pass	Fail
Stage 1	50,000	$\leq 1$	$\geq 5$
Stage 2	120,000	$\leq 6$	$\geq 13$
Stage 3	220,000	$\leq 14$	$\geq 15$

For AGR-2 fuel, the SiC defect fraction specification for particles after compacting is equal to that for the particles after coating, implying that the compacting process cannot produce any defects in the SiC layer or that the particles after coating must have, in effect, a lower defect fraction than specified.

The test data show no correlation of SiC defects with any coating process parameter. A general trend of lower defects with thicker SiC layers was found and is shown in Figure 9. For batches with an average SiC thickness  $\geq 34.5 \mu\text{m}$ , only one failed the SiC defect fraction specification, one was indeterminate and 13 passed. Conversely, for batches with an average SiC thickness  $< 34.5 \mu\text{m}$ , only two passed the SiC defect fraction specification, one was indeterminate and seven failed. Based on these results, the SiC thickness specification should be shifted from  $35 \pm 3 \mu\text{m}$  to at least  $37 \pm 3 \mu\text{m}$ .

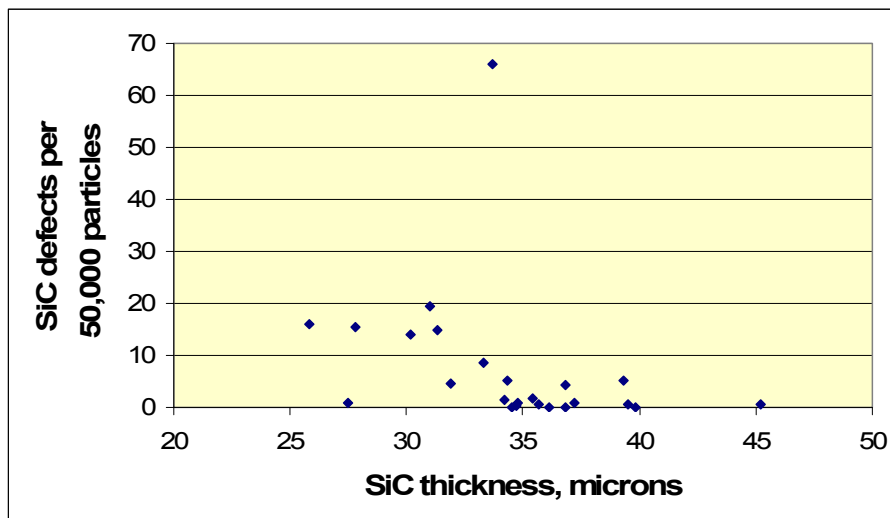


Figure 9. SiC defects versus layer thickness.

Improvements in particle upgrading may also have contributed to decreases in SiC defect fractions. Even though samples of particles from five of the first seven tests failed the defect fraction specification, particles from 11 of the last 12 tests passed. The primary changes made between these two groups of tests were changes in the particle upgrading methods. And while these changes apparently reduced SiC defect fractions, they did so at the expense of yield. Additional work is needed to determine defect fractions in rejected particle fractions toward the goal of improving overall yields from the coating process without compromising particle quality.

The intention of the AGR program is to reduce the SiC defect fraction in the future by a factor of 4. At this lower defect fraction, for the runs that had a SiC thickness greater than or equal to 34.5  $\mu\text{m}$ , four runs would have passed, four would have failed, and eight would have required analysis of more particles to determine acceptance. Additional analysis of some of these indeterminate batches is recommended. If a significant percentage fails the lower specification, failed particles should be further examined to seek to determine causes for failures. These efforts could lead to coater tests of additional nozzle designs or additional upgrading studies.

### 5.3 SiC Microstructure

The AGR-2 fuel specification contains a visual standard for evaluating SiC microstructure. The desirable fine-grained microstructure is typically achieved by limiting coating temperature. Partial dilution of the fluidizing gas with argon also results in a small grain microstructure.

The visual standard for SiC microstructure is shown in Figure 10. Figure 11 shows SiC microstructure for particles from three batches made with baseline conditions at B&W, three with argon-variant conditions at B&W, and examples of the AGR-1 baseline and Variant 3 particles.

All photos in Figure 10 were sized to the equivalent magnification of the standard in Figure 9. The grain sizes of AGR-2 baseline and argon-variant particles are very similar to each other and appear to be intermediate to the grain sizes of AGR-1 baseline and Variant 3 particles. The images below also show that the outer surface of SiC can vary considerably in appearance. As shown in Figure 11, though runs 93068 and 93069 were made with identical conditions of temperature and gas flow rates, the outer SiC surface of 93068 particles were smooth, while those of 93069 were very uneven.

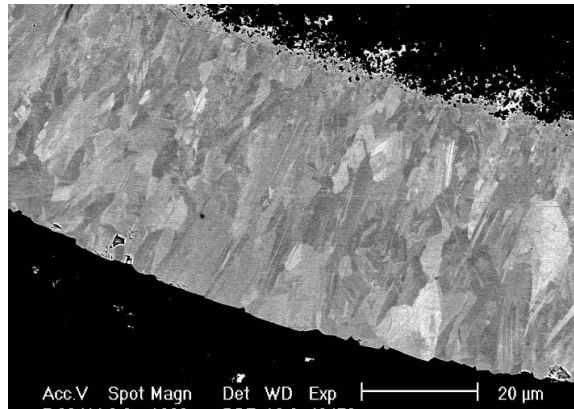
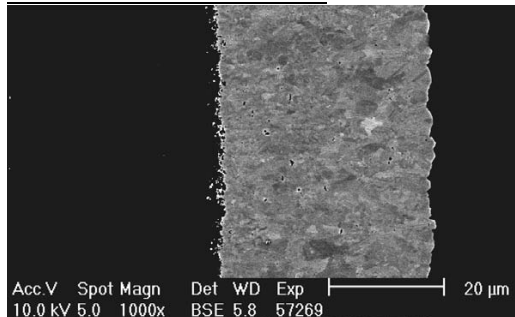
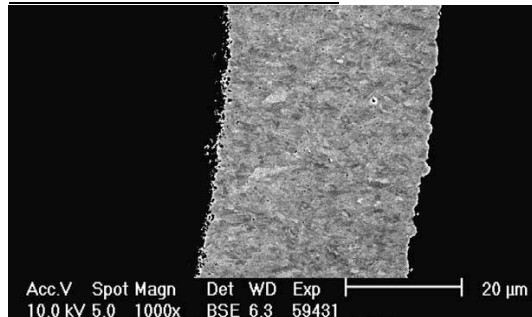


Figure 10. Visual standard for SiC microstructure showing particle with too large a grain size.

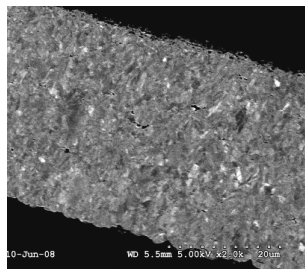
AGR-1 Baseline conditions



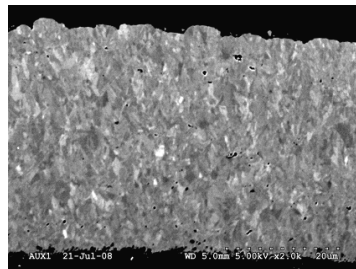
AGR-1 Variant 3 conditions



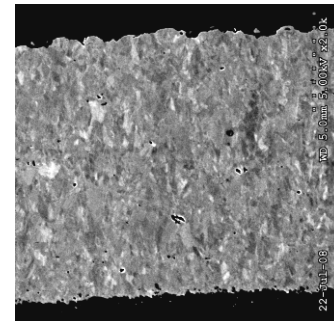
AGR-2 baseline conditions



Run 93060

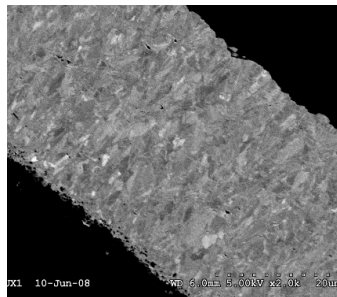


Run 93066

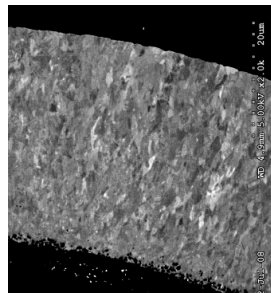


Run 93067

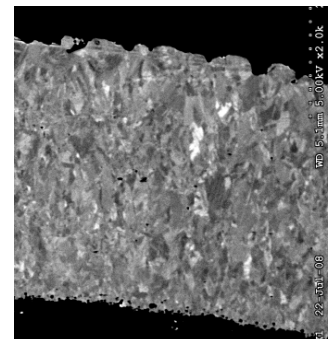
AGR-2 variant conditions



Run 93059



Run 93068



Run 93069

Figure 11. Comparison of SiC microstructure.

## 5.4 SiC Inclusions

A “gold spot” defect fraction specification was imposed on AGR-1 particles. Gold spots are discolorations seen at the outer surface of the SiC layer, appearing as yellow or gold areas. The SiC layer is translucent and the discoloration is due to delaminations, flaws, and/or inclusions of carbon or SiC soot, typically several microns thick, and extending circumferentially over a significant fraction of the particle. During development of the AGR-1 process, considerable effort went into examining particles for gold spots and seeking to reduce the gold spot defect fraction by changing gas flow rates and the ORNL coater nozzle design. Even with these efforts, the baseline AGR-1 particles barely met the specification of  $1 \times 10^{-3}$ , with 66 particles found with gold spots in a sample of 81,507 particles. No gold spots were seen in AGR-1 Variant 3 particles, which used partial argon dilution during SiC deposition. However, it was found from particle cross sections that this result for Variant 3 particles was not due to the absence of gold spots but because the smaller grain size SiC prevented the manifestation of the inclusions using the standard visual examination technique.

Images of ceramographic mounts of particles produced in early tests of the B&W coater showed an occasional inclusion, but large samples of particles were not examined for these inclusions prior to batch 93059. As of this time, three batches of test particles have been examined by ORNL. ORNL’s report, written by John Hunn, of results for the first two batches is given below. Results for the third batch (93066) were similar, with no inclusions found in a sample of 5415 particles.

ORNL analyzed G73F-NU-93059A (an AGR-2 Variant 1 Qualification TRISO coating run) and G73F-NU-93060A (an AGR-2 Baseline Qualification TRISO coating run) for SiC soot inclusions using the following procedure.

Particles were pour sampled from the 30 g samples supplied by B&W. Six 1.25 in. cylindrical molds were filled with a single layer of particles and covered by 2-parts epoxy to form a mount. The number of particles analyzed was calculated by weighing particles in mounts and dividing by an estimated average particle weight obtained from layer thickness and density data.

Mounted particles were ground and polished to close to mid plane. These cross sections were then imaged using a  $9 \times 12$  tiled array to cover each mount (108 images per mount). The images were then manually inspected for soot inclusions in the SiC layer using bright field reflected light. If a continuous line could be seen in the SiC layer that extended for more than a few degrees arc, it was counted as a defect. Spots that appeared due to porosity, pullout, or poor polish were not counted. Note that the polish was minimized to maintain a planar surface. This resulted in some poorer polished particle around the perimeter of the mount, in some cases. Any unusual feature was noted and reanalyzed by reviewing the images and/or reanalyzing them using the optical microscope at higher magnification and other illumination conditions.

The AGR-2 Variant 1 sample (93059A) showed 0 defects out of 6257 particles. This corresponds to a defect fraction<sup>a</sup> of  $<4.8\text{e-}4$ . The AGR-2 Baseline sample (93060A) showed one defect out of 5917 particles. This corresponds to a defect fraction of  $<8.1\text{e-}4$ . These defect fractions assume that a defect is defined as a soot inclusion that can be seen using bright field under the conditions used and that the single examination of a mid-plane cross section is sufficient to fully analyze the sample. In reality, some statistical correction should probably be applied to the analysis to account for the probability that a soot inclusion defect may exist in some of the analyzed particles in a location not exposed by the mid-plane cross section. Based on soot inclusions and gold spots observed

---

a. Reported defect fractions for 93059A and 93060A are at the 95% confidence level.

on other TRISO particles, which usually cover at least half the particle, the probability of missing a defect using the single mid-plane examination may be fairly low. In addition, no evidence was seen in these two B&W samples that there is a population of smaller sized inclusions that would require examination using multiple polish planes. A rough estimate of the effect of missing a defect in 10% of the examined particles would be to increase the 95% confidence defect fraction to  $9\text{e-}4$  for the AGR-2 baseline particles.

Soot inclusions were also looked for at the IPyC/SiC interface. In some development batches for AGR-1, use of an over fluidized condition was tried at the beginning of the SiC run in order to obtain better fluidization at the end of the run. These tended to produce goldspot defects related to thick soot inclusions at or near the IPyC/SiC interface. A number of particles with pullout/crumbling at the interface were noted. However, after closer examination on the microscope, it could be seen that these regions were significantly different from those related to earlier observed goldspot/soot inclusions. In the B&W particles, the region is bridged by “good” IPyC. In the old gold spot particles, the region is bridged by SiC. The crumbled interfaces in particles noted in the B&W samples appeared to be related to pullout of the IPyC as opposed to a soot layer between the IPyC and SiC, which is usually accompanied by SiC infiltration through the porous soot.

The one particle that was identified as a SiC soot inclusion defect is shown below in Figure 12. A line can be seen at the same radius in several positions around the particle (1, 8, 9, and 11 o’clock). One might argue against counting this as a defect because it actually appears to be pull-out associated with a weakened band of SiC that might otherwise have only appeared as a dark field anomaly, as opposed to a layer of low density soot of any appreciable thickness.

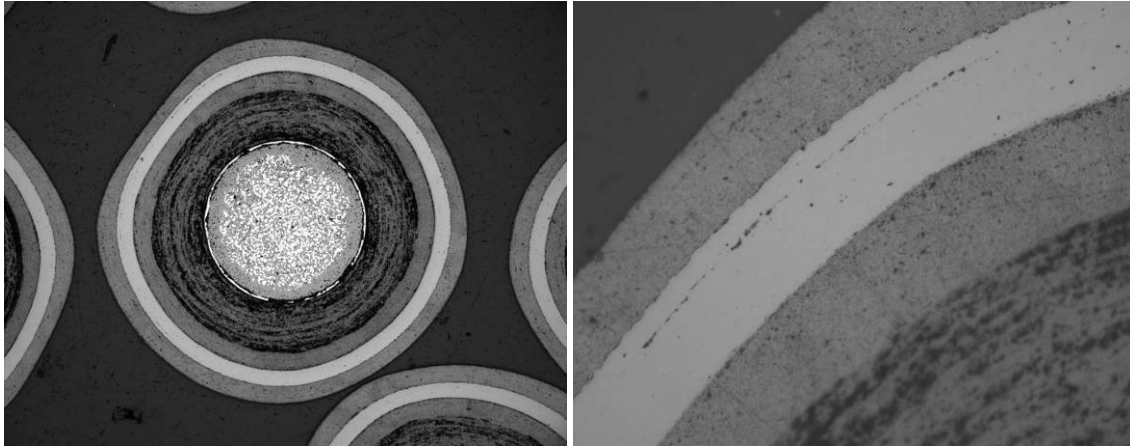


Figure 12. The one SiC inclusion found in sample of 93060 particles.

ORNL is currently analyzing additional samples of particles produced in the B&W coater, including particles from run 93069 and from each of the LEU batches produced for AGR-2. Initial results show that particles from run 93072 do have a significant fraction of inclusions. The SiC layer of this run is anomalous in that it was deposited with an MTS concentration of 2.15%, slightly outside the process specification range of  $1.5 \pm 0.5\%$ .

## 5.5 SiC and OPyC Aspect Ratio

The AGR-2 fuel specification requires that not more than 1% of the SiC-coated particles have an aspect ratio greater than or equal to 1.14. Asphericity in particles results in stress concentrations that can contribute to failure of the SiC layer.

Mean and upper critical limit aspect ratios are shown in Figure 13 for the 11 coater qualification runs, for both the SiC and OPyC layers, after sieving and tabling. Particles from all runs are well under the specification limit. No difference is seen in the aspect ratios of particles from runs using baseline conditions compared to those using variant conditions. Runs with higher SiC aspect ratios generally have higher OPyC aspect ratios but Figure 13 shows several exceptions to this observation.

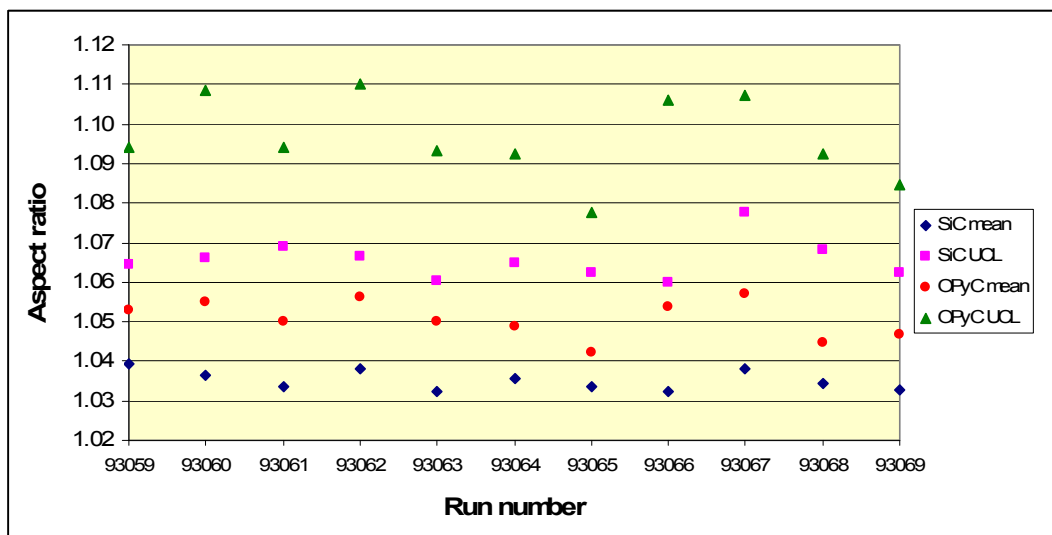


Figure 13. SiC and OPyC aspect ratios.

## 5.6 Selection of Variant SiC Conditions

Of the possible variants to pyrocarbon and SiC layer depositions, the one deemed most attractive from a production perspective is that of increasing the deposition rate and decreasing the deposition temperature of the SiC layer. Doing so would decrease the production cycle time, increase the usable life of coating furnace components, potentially reduce nozzle accretions, and reduce the thermal degradation of IPyC anisotropy.

The SiC deposition conditions explored by ORNL for AGR-1<sup>12</sup> and investigated by the Japan Atomic Energy Research Institute (JAERI)<sup>11</sup> were considered. The JAERI research indicated that the MTS concentration could be increased to 3 mol% without a degradation in the SiC density or crystalline structure by the incorporation of approximately 20–40% argon in the fluidizing gas. Data were extracted from both reports and plotted in Figure 14.

Curves for 0.4%, 2%, and 3% MTS were taken from the JAERI report and the curve for 1.4% MTS is a mathematical interpolation of the JAERI data. The curves represent what is thought to be the optimal conditions for SiC formation without having an excess of either carbon or silicon in the crystal structures. Deviation from the curves may lead to nonstoichiometric Si:C ratios in the SiC. The actual position and shape of the boundaries have not been confirmed, so some caution is warranted in using the graphs to guide experimentation.



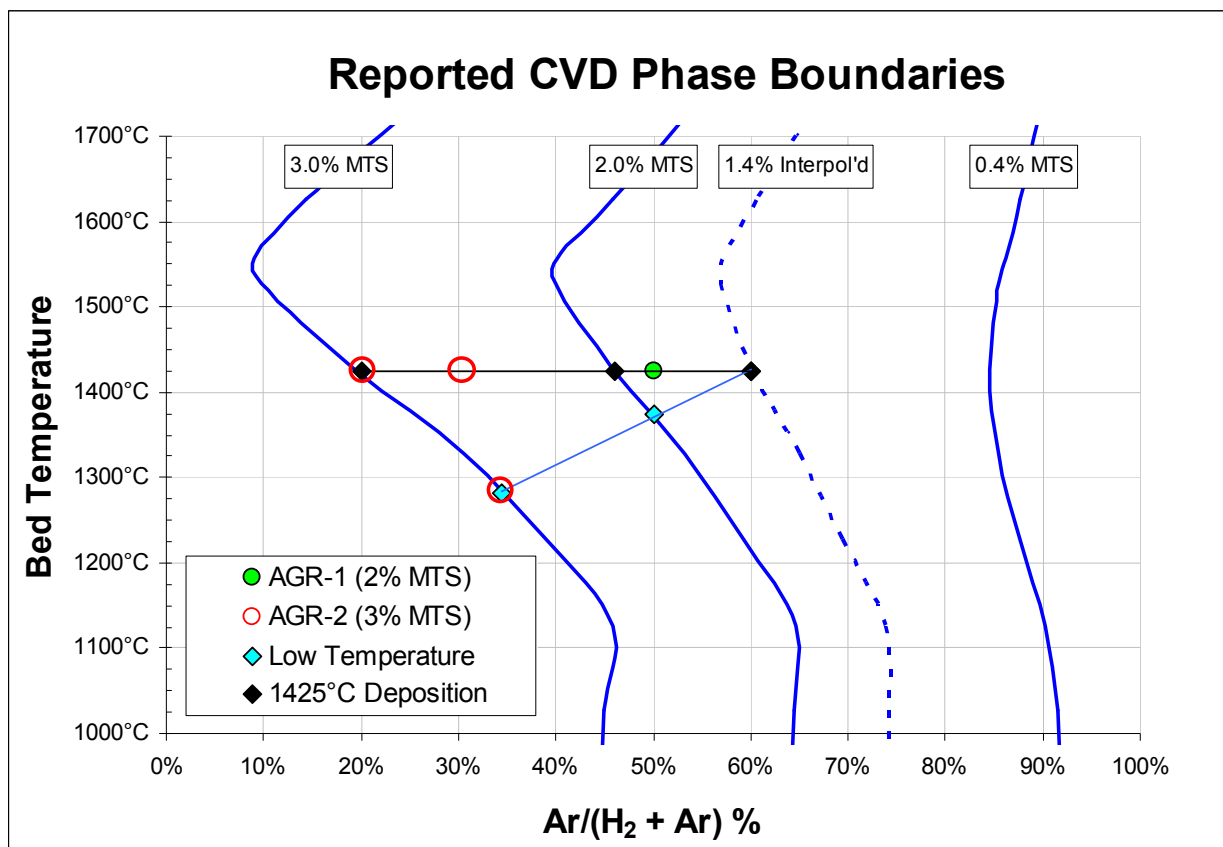


Figure 14. SiC phase boundaries and target operating points.

To determine SiC variant coating conditions, an initial test matrix was set up to include three points from 1.4 to 3% MTS at 1425°C and at identical concentrations, but lower temperatures as shown by the connecting lines on the graph. It was found that acceptable SiC could be achieved at 3% MTS and 20% argon, but the low temperature case of 34% argon and approximately 1280°C was not acceptable. The MTS conversion and SiC deposition efficiencies were low and the SiC density was unacceptably low at 3.145 g/cc. 2% MTS conditions were not tested because of the success with 3% MTS.

Hydrogen gas flow rates during the baseline SiC deposition are near 189 standard liters per minute (slpm) and limited in flow primarily by the offgas temperature in the furnace exhaust. The gas flow rates for the argon variant were selected to achieve similar fluidization to that achieved with hydrogen in the baseline case. This was done to minimize changes to the bed fluid dynamics while testing the argon variant. Argon, being 20 times denser than hydrogen and more viscous, has approximately twice the fluidizing potential as hydrogen gas. The argon and hydrogen gas flow rates were selected to be approximately 37 and 85 slpm, respectively, for a total gas flow rate of about 122 slpm.

Based on the results of these few runs, conditions selected for the AGR-2 argon variant were 30% argon and 3% MTS. These are successful conditions, but room for improvement remains. Gas flow rates changes should be investigated to improve bed fluidization during SiC deposition and to shorten deposition times. Tests should also be conducted to determine if lower temperatures and higher total gas flow rates can be used while still achieving a high MTS conversion and good SiC density.

## 6. OUTER PYROLYTIC CARBON LAYER

The purposes for the OPyC layer include (a) acting as a final barrier in the particle to release of gaseous fission products, (b) maintaining the SiC layer in compression during irradiation, (c) protecting the SiC layer from impurities and mechanical damage during handling in subsequent fabrication steps, and (d) providing a bonding surface for compact matrix. Specifications for the OPyC layer include the average thickness, the lower critical limit thickness, the average density, upper and lower density critical limits, mean anisotropy, upper anisotropy critical limit, and missing OPyC layer defect fraction. The OPyC surface connected porosity, while not a specification, is also of interest because some historical data show a correlation between OPyC surface connected porosity and OPyC failures during irradiation.

This section discusses results of coater tests for the OPyC layer, compares them to AGR-1 results, and compares them to results for the IPyC layer.

### 6.1 OPyC Density

Thickness and density specifications for the OPyC layer are identical to those for the IPyC layer. Thus, coating conditions for these two layers are similar but not identical due to the difference in IPyC- and OPyC-particle diameter. Figure 15 shows IPyC and OPyC density versus bed temperature for both the B&W and AGR-1 coaters. A higher temperature is required for the OPyC layer than the IPyC layer to achieve the same layer density. Also, the change in density with temperature is greater for the OPyC layer than the IPyC layer. Thus, the temperature range that will result in acceptable OPyC densities is narrower than that for the IPyC layer.

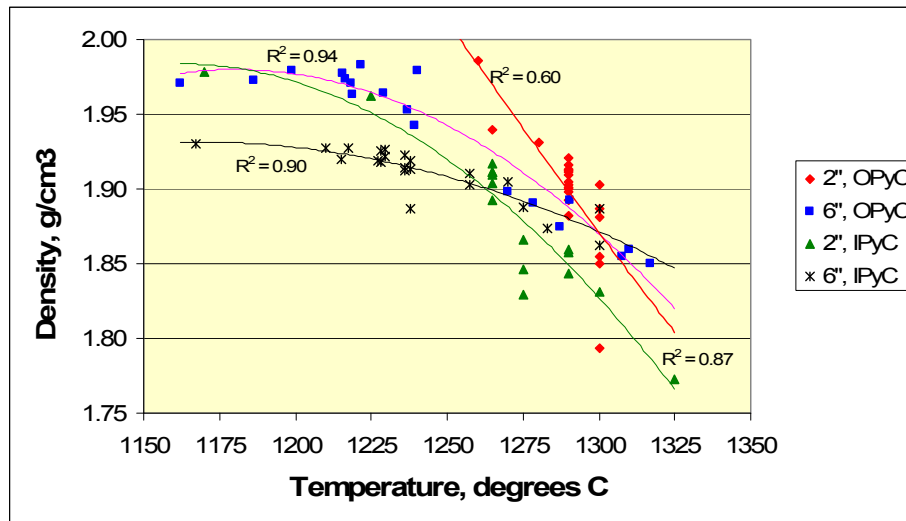


Figure 15. Comparison of pyrocarbon density versus bed temperature data.

Figure 16 shows pyrocarbon densities plotted against both bed and control temperatures for the B&W coater. Both Figures 15 and 16 show considerable scatter in densities of particles with OPyC layers applied with the same temperature. This uncertainty limits the acceptable OPyC control temperature that will result in specification densities to a very tight range, approximately 1335–1360°C. Later test results showed more run-to-run consistency in pyrocarbon densities, suggesting that the scatter in the data plotted in Figures 15 and 16 was in large part due to variations in charge size, charge mass, and other coating parameters that were changing from run-to-run during the early tests. Still, to avoid the possibility of thermocouple drift that could result in particles missing the density specification, a review of ways to improve and/or provide redundancy to coater temperature measurements is recommended.

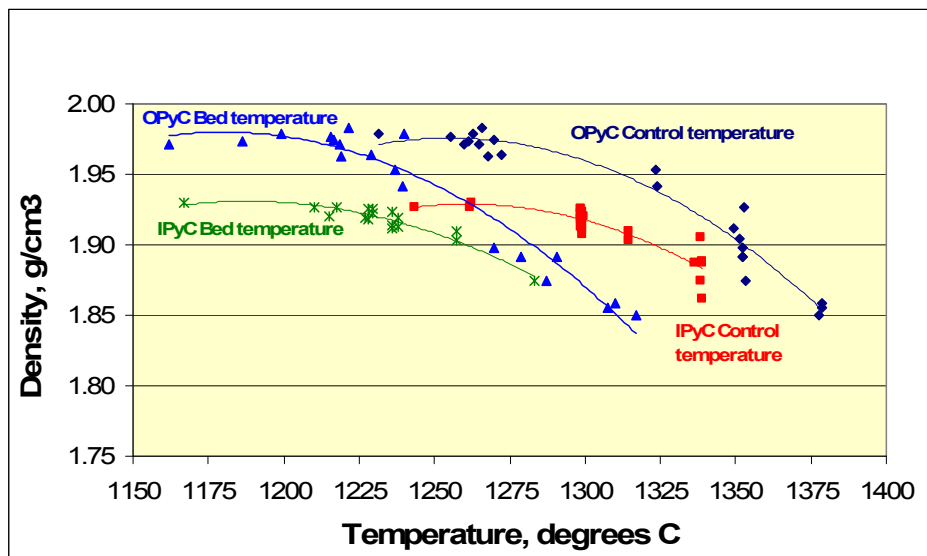


Figure 16. Pyrocarbon density versus temperature for B&W coater.

## 6.2 OPyC Anisotropy

OPyC anisotropies are plotted versus bed temperature in Figure 17 and versus coating rate in Figure 18. For reference these plots also show IPyC anisotropies. For runs that had no internal thermocouple, the bed temperature was estimated from the layer density. Anisotropies plotted are the “equivalent BAF<sub>o</sub>” defined as  $1 + 3 \times \text{diattenuation}$ , in order to better compare these values to historical data. True anisotropy values are lower than those shown, i.e.,  $1 + 2 \times \text{diattenuation}$ .

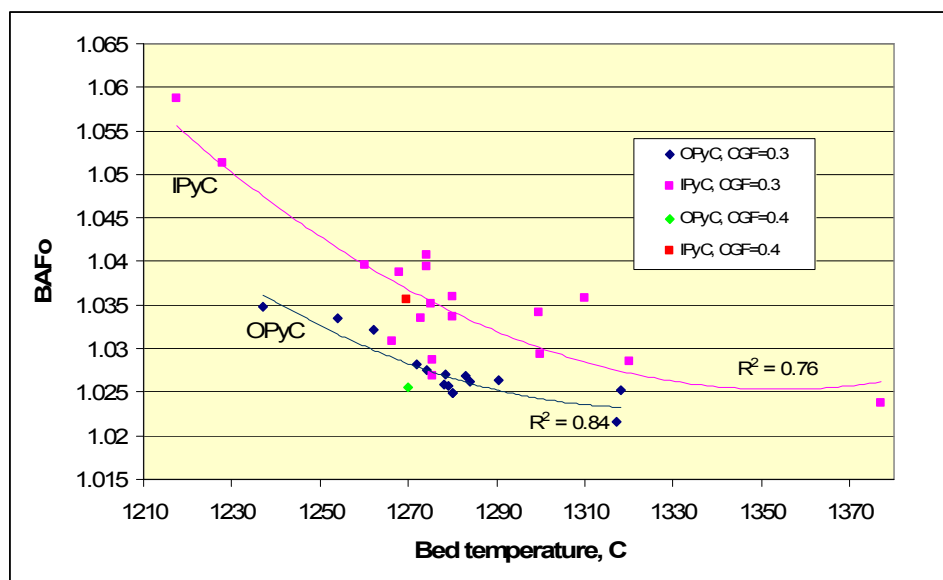


Figure 17. Pyrocarbon equivalent anisotropies verses bed temperature for B&W 6-inch coater.

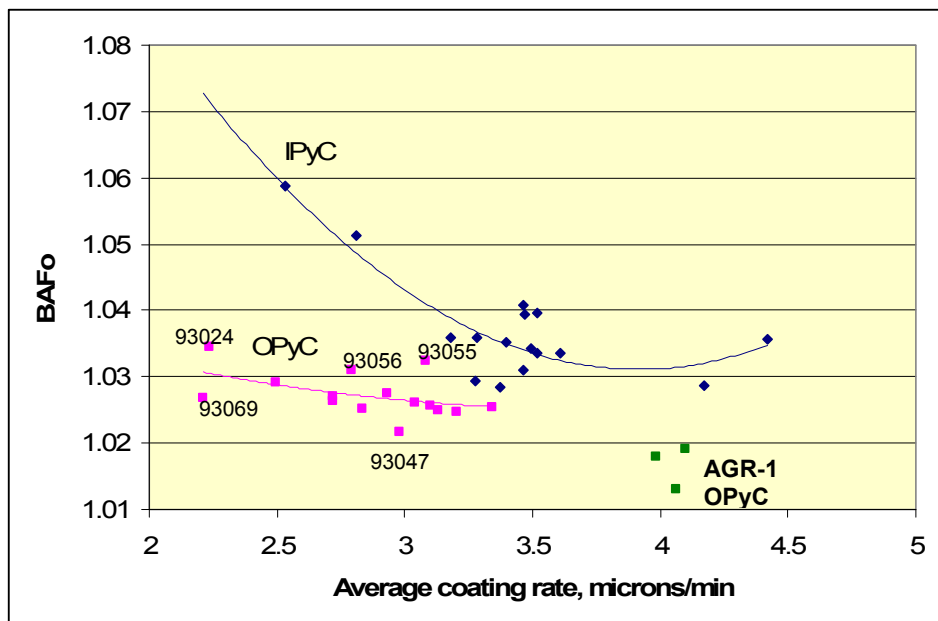


Figure 18. Pyrocarbon anisotropy versus coating rate.

For a given temperature or coating rate, the OPyC anisotropy is lower than the IPyC anisotropy. In the temperature region of most interest, this difference amounts to about 0.008 BAF<sub>o</sub> units. A possible explanation for part or all of this difference is the change in IPyC anisotropy during SiC coating. A second reason that OPyC anisotropies are lower than IPyC anisotropies for a given coating run is that the OPyC layer is applied using a higher temperature.

At the OPyC coating temperature corresponding to achieving a layer density of 1.90 g/cm<sup>3</sup>, the OPyC density was typically 1.027, well under the specification limit of 1.035.

Only one test was made with an OPyC coating gas fraction greater than 0.32, and as shown on Figure 17, this run, which used a coating gas fraction of 0.4, resulted in a lower anisotropy. Additional tests at coating rates in the range of 0.35–0.4 are recommended, should it be desired to reduce OPyC anisotropy.

As was the case for IPyC anisotropy, OPyC anisotropies are higher than those measured for AGR-1 particles. Limitations in flow rate in the B&W offgas system prevented achieving the AGR-1 OPyC coating rates (at equivalent coating gas fractions). Modifications of the B&W coater offgas system could be made to achieve higher flow rates.

Comparing Figure 17 and Figure 18, OPyC anisotropy correlate much better with temperature ( $r^2 = 0.84$ ) than coating rate ( $r^2 = 0.23$ ). Of the five data points that deviate most from the trend line (identified by run number in Figure 18), the deviations in anisotropy for four of these can in part be explained by temperatures experienced in these particular tests. The uniqueness about the run represented by the fifth data point, 93069, is that it had an unusually high pressure drop across the gas nozzle and particle bed due to constrictions in several nozzle orifices as a result of SiC deposits. Figure 19 shows the relationship of anisotropy to the coater pressure drop. The data point for the run with this high pressure drop seems to correlate with the data from three of the other runs (93024, 93055 and 93056) that do not fit the correlation with coating rate. Pressure may have an effect on anisotropy, although the exact nature of that relationship is not yet clear.

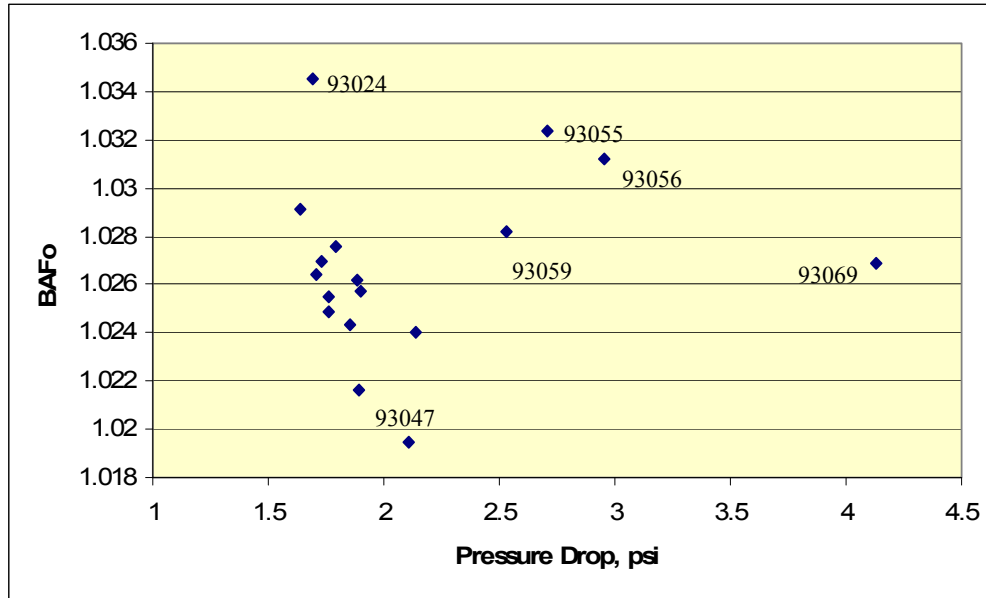


Figure 19. Relationship of OPyC anisotropy to pressure drop across coater.

### 6.3 Missing OPyC Layers

The specification for missing OPyC layer defect fraction is  $\leq 3 \times 10^{-4}$ . No particle with a missing OPyC layer was found in any of the particle batches produced this year. For many of the tests, only about 1,000 particles from each batch were examined, but for each of the 11 qualification tests (93059–93069), about 16,000 particles were examined for missing OPyC layers.

### 6.4 OPyC Surface Connected Porosity

Bullock<sup>13</sup> documents data showing a relationship between percent OPyC failure during irradiation and OPyC microporosity. His report shows data points for loose particles fabricated by General Atomics and irradiated in 11 capsule tests. Some data for particles with porosities as low as  $\sim 0.5 \text{ ml/m}^2$  show very low failures, while other data for particles with porosities of  $0.3\text{--}1.2 \text{ ml/m}^2$  show high levels of failures, increasing with decreasing porosity. The report theorizes that the data on this plot can be divided into three regions identified by different pyrocarbon structures. For particles with low porosities, if they have small isotropic growth features the failure rate is low, but if they have anisotropic growth cones, the failure rate is high. From all indications of coating conditions, the B&W particles should have pyrocarbon microstructure corresponding to the region with low failures. However most measurements of B&W particles show surface connected porosities of  $0.4\text{--}0.8 \text{ ml/m}^2$ . ORNL measured OPyC surface connected porosity of German particles to be  $0.685 \text{ ml/m}^2$  for  $250\text{--}10,000 \text{ psi}$  and  $1.1 \text{ ml/m}^2$  for  $250\text{--}60,000 \text{ psi}$ . It was noted that the increase in porosity of the German particles at higher pressures was unusual compared to AGR-1 particles.

While OPyC surface connected porosity is not a particle specification, the AGR-1 fuel specification showed a target value of greater than  $1.3 \text{ ml/m}^2$  as desirable and, hence, an average coating rate close to  $4 \text{ }\mu\text{m/min}$  was used to produce AGR-1 particles.

OPyC surface connected porosities from B&W (6-inch-diameter coater) tests are shown on Figure 20, along with IPyC porosities and AGR-1 (2-inch-diameter coater) OPyC porosities.

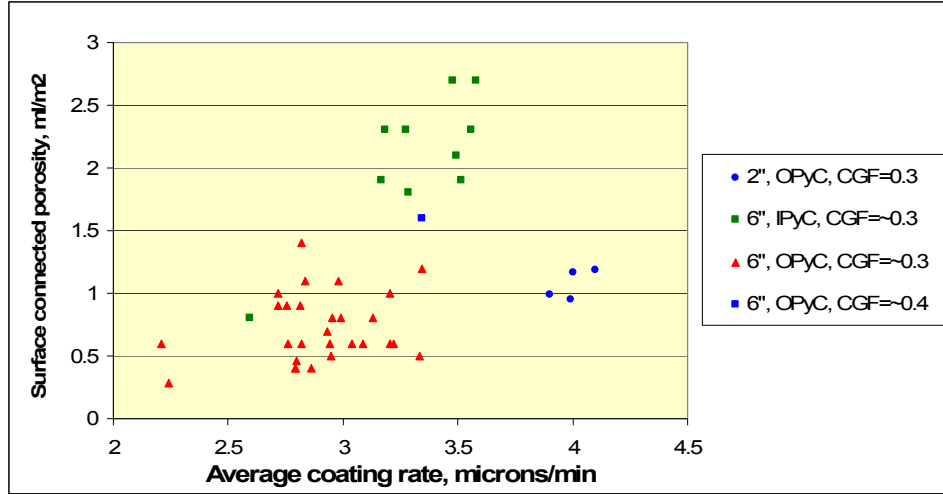


Figure 20. Surface connected porosity versus average coating rate.

While Figure 20 shows a general trend of increasing porosity with increasing coating rate, the scatter in the B&W OPyC data is large. All of the data points indicating OPyC porosities of 1.0 ml/m<sup>2</sup> or higher are from early tests. Much of the remaining data is consistent with porosities measured for AGR-1 particles, although porosities are lower due to the layer being applied at a lower coating rate.

Hot samples of OPyC particles were taken in three coating runs, to determine whether the interaction of particles during cooling in the coater plus the subsequent handling of the particles during unloading and upgrading affected the OPyC surface connected porosity. Results are shown in Table 4. In all cases the porosity of the hot sample was higher than the bulk sample after sieving and tabling. The differences observed indicate some surface compaction may occur as the bed cools under fluidizing conditions or are upgraded by sieving and tabling, leaving the bulk of the OPyC layer with a higher connected porosity than the outer surface.

Table 4. Effect of cooling and upgrading on OPyC porosities.

Run	OPyC Surface Connected Porosity (ml/m <sup>2</sup> )	
	Hot Sample	Upgraded Sample
93063	0.9	0.8
93065	0.7	0.4
93069	0.9	0.6

OPyC surface connected porosities measured by ORNL are lower than those for samples from the same batches measured by B&W, as shown in Table 5. Both ORNL and B&W use porosimeters manufactured by Quantachome, although B&W has a newer model with an updated version of software. ORNL has reviewed and compared raw data from both laboratories and concluded that the differences in porosity values are due to differences in the instruments. Additional efforts including discussions with the instrument manufacturer are needed to resolve the discrepancies in these readings.

Table 5. Comparison of ORNL and B&W porosity measurements.

<b>Run #</b>	<b>ORNL porosity (ml/m<sup>2</sup>)</b>	<b>B&amp;W Porosity (ml/m<sup>2</sup>)</b>
93031	0.456	0.9
93044	0.397	1.0
93046	0.369	1.0
93059	0.390	0.5
93060	0.366	0.7

## 7. PRESSURE FLUCTUATION DATA ANALYSIS

Pressure fluctuations and total system back pressure have been monitored on the 6-inch coater throughout the development of the coating parameters as a tool to understand the impact of process changes on bed hydrodynamics and particle properties. Pressure fluctuations are caused by the movement of gas bubbles and the particle bed within the coater, which are functionally related to gas and particle properties. Because particle and gas properties are strongly linked to the pressure fluctuations, one would expect the structure of the pressure fluctuation signal to reveal information about particle properties. Early investigations of the pressure fluctuations focused primarily on defining process parameters that would provide adequate fluidization of the particle bed, but also found evidence that coated particle aspect ratios could be estimated from the amplitudes of the peaks on a power spectral density plot.<sup>5</sup> The investigation into possible relationships between particle properties and the structure of the pressure fluctuations has continued. The pressure sampling rate was decreased from 500 to 400 Hz and the sampling time increased from 5 to 8 seconds to ensure that the pressure fluctuation data were sufficiently representative for the coating while keeping the data file sizes manageable.

Data are collected at three intervals during the each coating layer deposition. The first is approximately one minute after coating gas flow is initiated, the second near the midpoint of the deposition, and the third approximately one minute before the coating gases are terminated.

When the bare kernels are charged to the coater vessel, the particle bed is very shallow. Consequently, the initial flow patterns are not well developed and pressure fluctuations are somewhat unstructured. During the course of buffer deposition, the volume of the bed expands three-fold as the particles increase in diameter and the pressure fluctuation pattern becomes more structured. Figure 21 shows representative pressure fluctuation curves during buffer deposition and Figure 22 shows the short-time Fourier transform (STFT) plot of the pressure signals, illustrating the change in the characteristic frequency of the pressure fluctuations over the sampling period. A downward shift in the dominant frequencies is observed as the buffer coating accumulates and the pressure fluctuations signals become more regular and predictable.

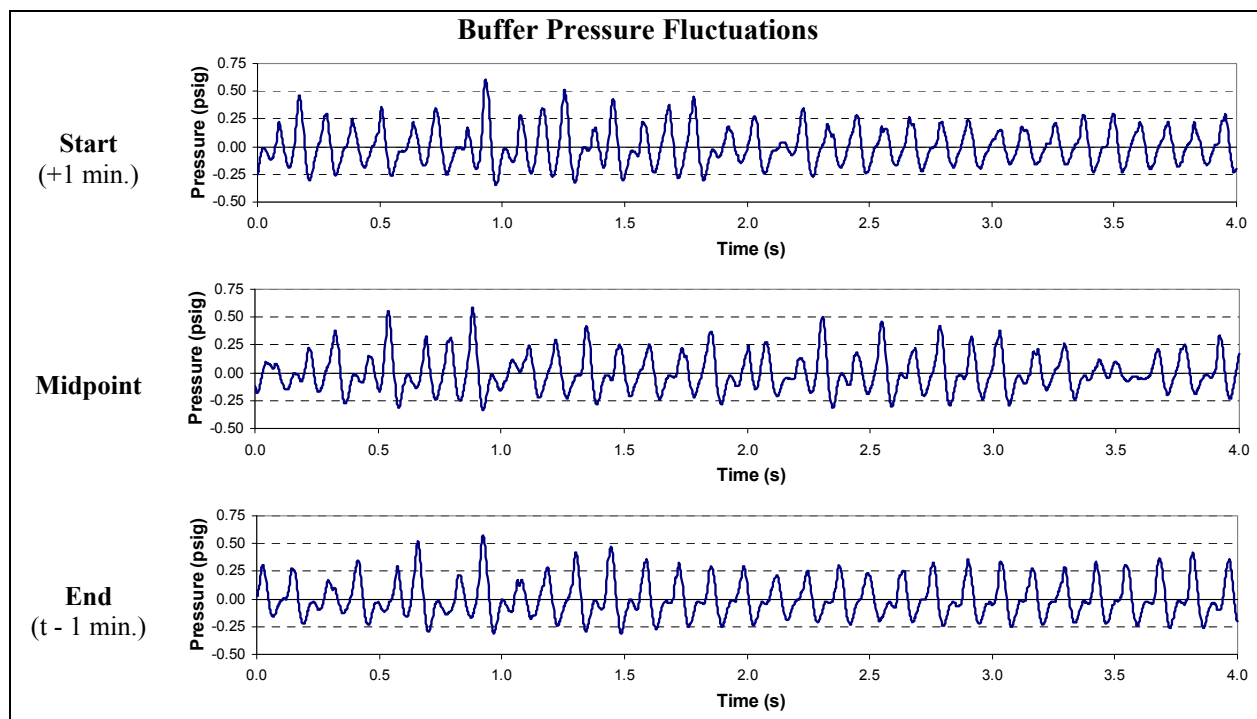


Figure 21. Plots of pressure fluctuations during the course of buffer deposition.



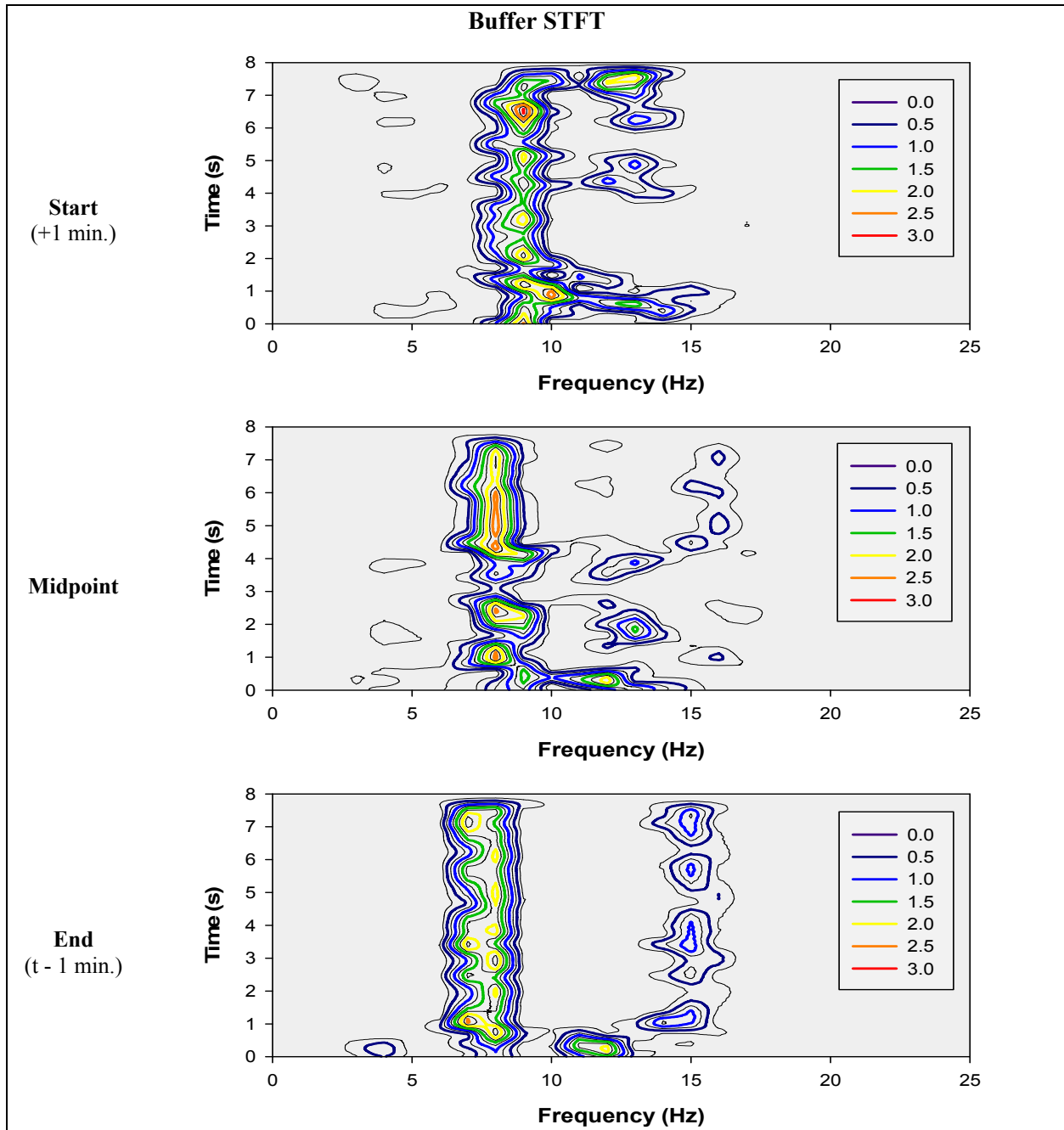


Figure 22. STFT plots of pressure fluctuations during the course of buffer deposition.

The fluctuation patterns manifested at the end of buffer deposition and during IPyC deposition as shown in Figure 23 are believed to be a manifestation of a desirable fluidization regime within the bed characterized by two local maxima and minima per cycle. Modeling completed by ORNL<sup>14</sup> has been used to interpret the bed behavior as it correlates with the observed structure (see Figure 24). The MFIX model predicts that the rapidly expanding gases above the gas injection nozzle form a repeating succession of large and small bubbles that shed (separate) from the gas nozzle, rise through the bed, and erupt at the surface. The bubbles form an intermittent spout near the centerline of the bed through which particles are transported from the lower portions and ejected out the top of the bed.

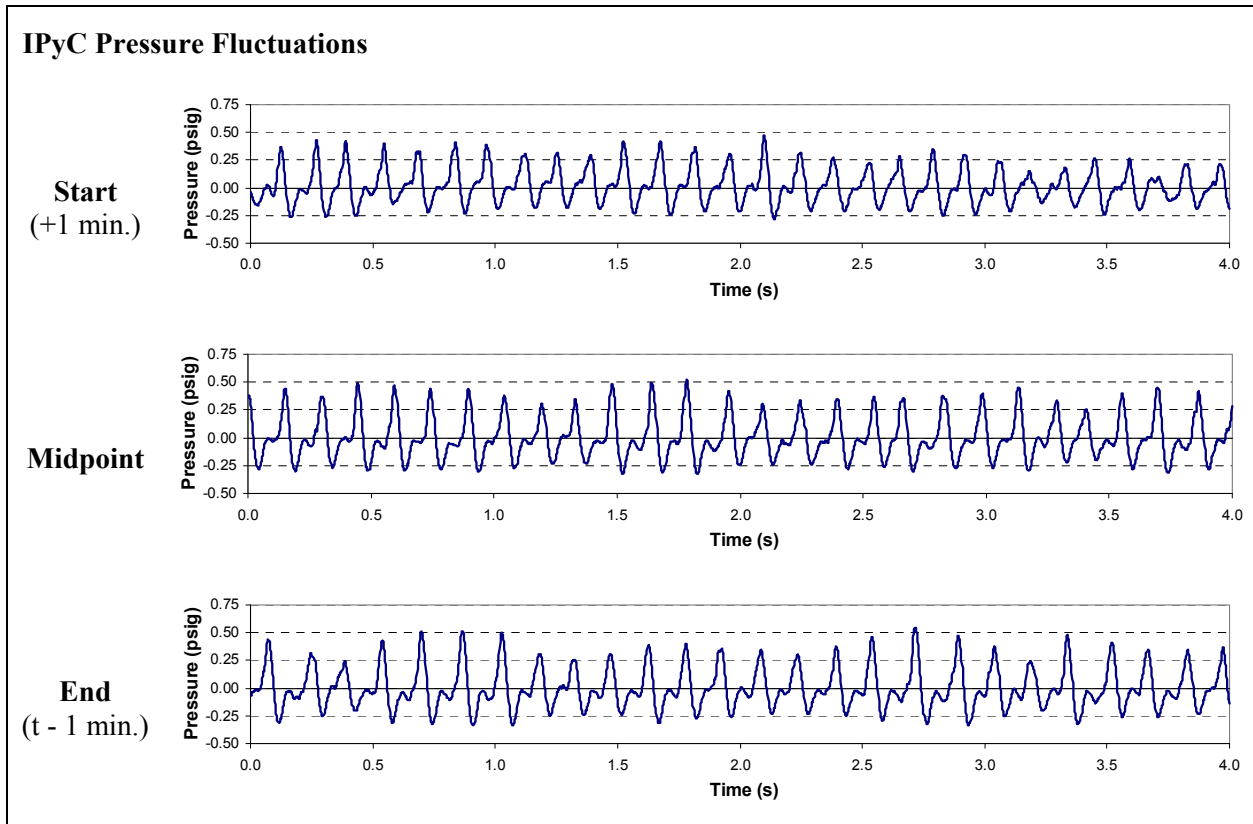


Figure 23. Plots of pressure fluctuations during the course of IPyC deposition.

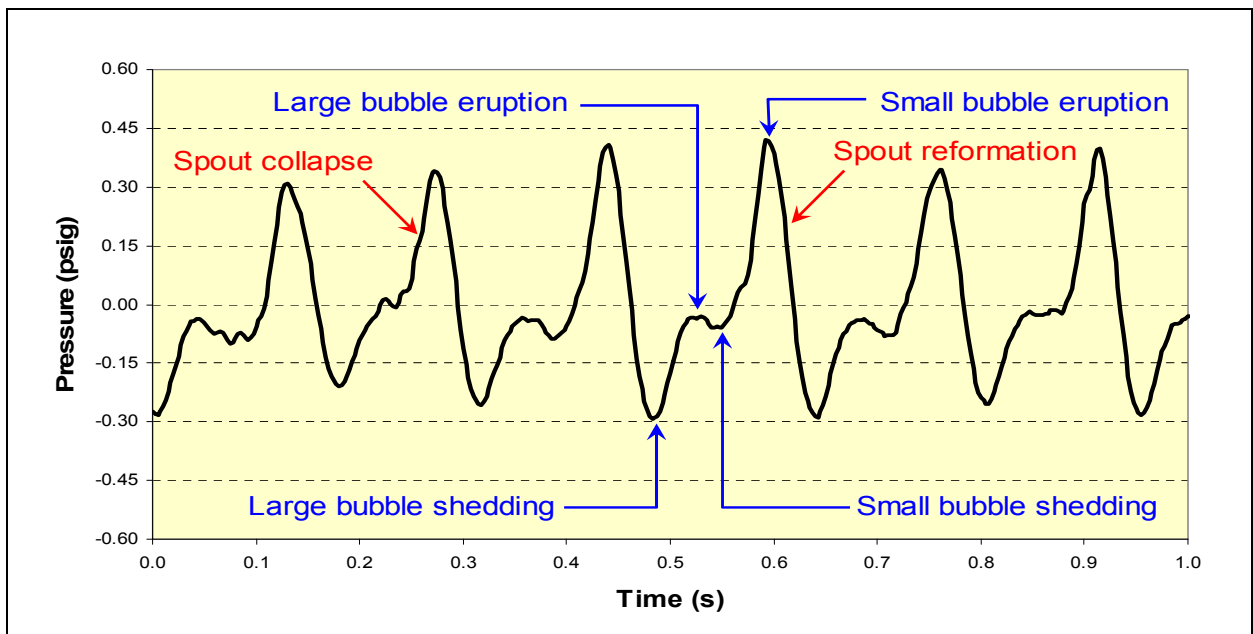


Figure 24. Interpretation of features on a pressure fluctuation plot.

Two additional means of analyzing the pressure fluctuations have been added in the past year: Hurst exponents and Strange attractors. The Hurst exponent is estimated from the slope of a “rescaled range analysis” plot (a.k.a. Pox plot; Figure 25) taken for various lag ranges. Slopes near unity indicate a high “persistence” in the data trend (the trend is preserved when data are extrapolated), while slopes near zero indicate an antipersistence (the trend is opposite of what would be predicted by data extrapolation). Strange attractors are produced when the pressure transducer data are plotted against themselves with a lag (offset) of several data points as seen in Figure 26.

Strange attractors are pseudo-phase plots produced when the pressure transducer data are plotted against themselves with a lag (offset) of several data points (Figure 26); determined by two points on an autocorrelation plot to maximize and minimize “mutual” information. Figure 26 shows the Strange attractors for buffer deposition corresponding to the pressure fluctuations in Figure 21 and Figure 22. The upper row in the figure holds the plots exhibiting a maximum in mutual information and the lower row has plots exhibiting a minimum in mutual information. Both show a progression of the pressure signals toward a higher degree of structure and regularity as the buffer deposition progresses. Maximum mutual information corresponds approximately to a lag where the autocorrelation plot is zero and minimum mutual information occurs approximately where the autocorrelation reaches the first positive maximum (Figure 27), which also corresponds to the average cycle period ( $\text{lag}/400 = \text{period}$ ). Strange attractors are useful in that they provide a visual representation of the amplitude of the pressure fluctuations by the radial dimension of the plot, the variability of the signals by how well the successive cycles overlay each other, and a qualitative indication of structure in the signal. The upper pattern in Figure 26 for the bare kernel is similar to that produced by a stable spouted bed and the pattern for the particle at the end of buffer coating is more reminiscent of an “unstable” or pulsating spouted bed.

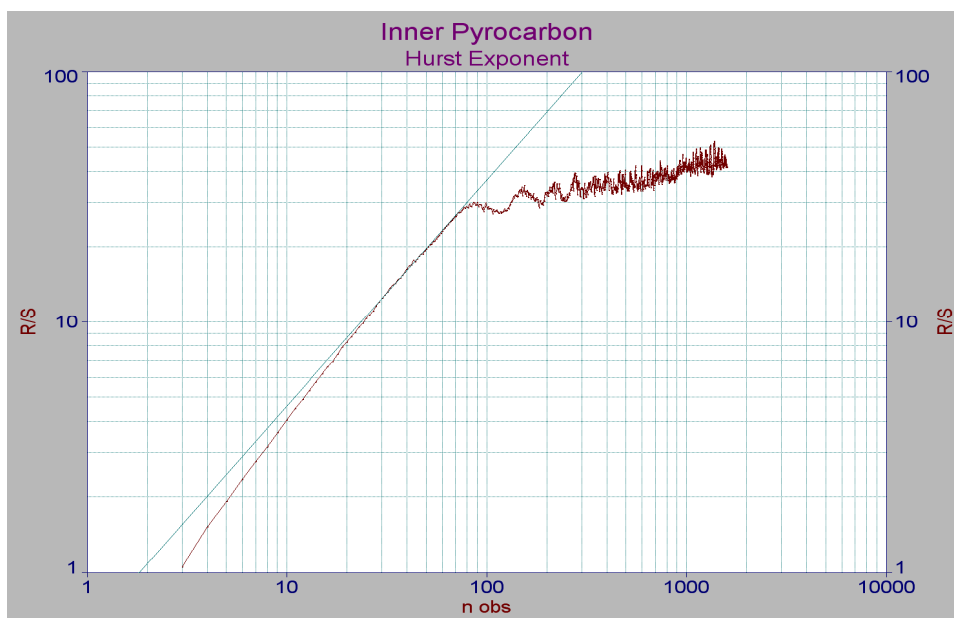


Figure 25. Rescaled range analysis (Pox) plot used for determining Hurst exponents.

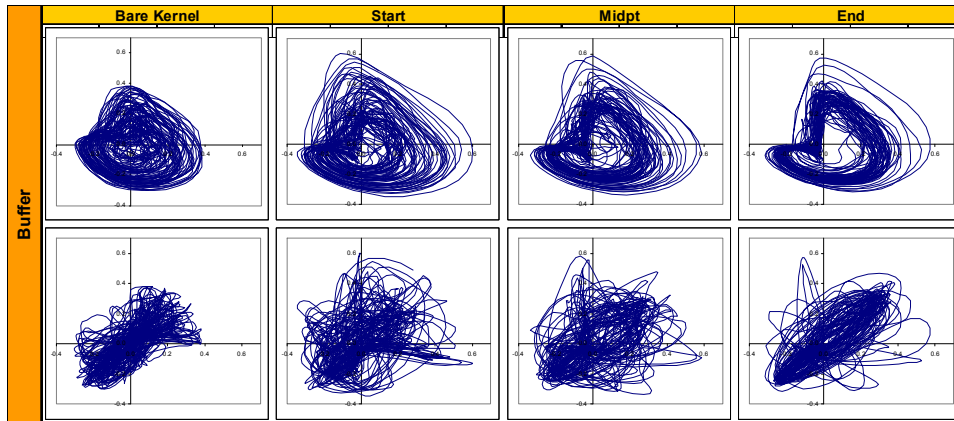


Figure 26. Representative Strange attractor plots for buffer deposition.

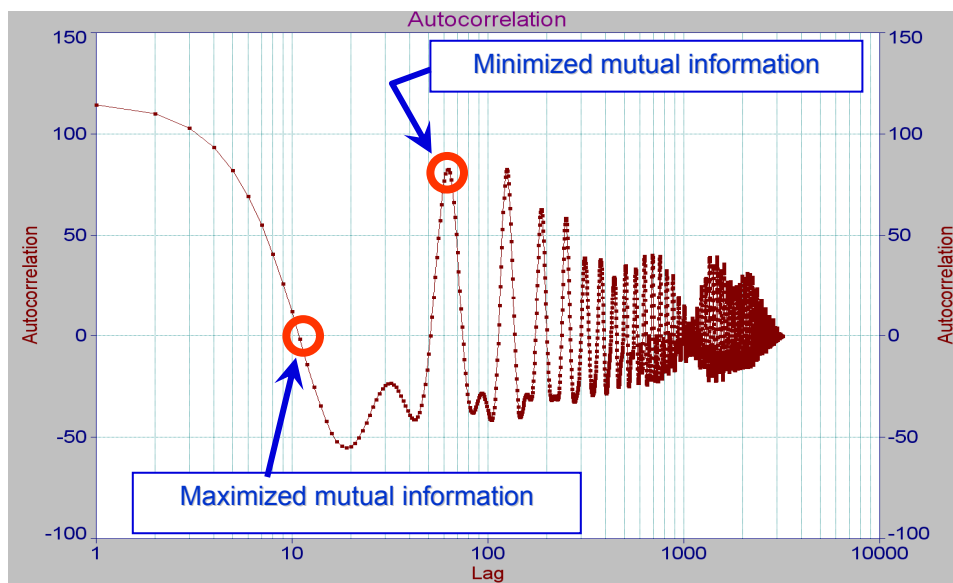


Figure 27. Autocorrelation plot showing features corresponding to maximum and minimum mutual information points on Strange attractor plots.

A change in the bed pressure fluctuation signal for OPyC layers applied following SiC deposition using an argon-hydrogen variant flow sheet was first observed in the Strange attractor plots. This change is persistent throughout the deposition of the entire OPyC layer, suggesting that the change is not caused by either surface or bulk properties of the particles, but related to the coater vessel. It has been observed that the nozzle accretions from the argon variant are generally smaller in height and have more severely narrowed orifices than accretions formed during a baseline run. The different accretion characteristics are believed to be the result of differences in the nozzle operating temperature. The argon variant uses less gas flow to achieve the same degree of bed fluidization as the baseline and is less able to sweep heat away from the nozzle. Although the greater degree of occlusion in the accretions would increase the gas velocity exiting the nozzle, it does not impact the superficial gas velocity through the remainder of the bed. The higher gas velocities could result in greater “jet” penetration into the bed and extend the length of a stable gas spout. Another possibility is that the nature of the SiC fouling on the vessel wall may differ with the two deposition mechanisms, which may change the particle-wall sliding friction and, consequently, the bed circulation rate. Bed circulation directly impacts the size of bubbles that form and gas spout stability, which are manifested in pressure fluctuation signals.

Of the possible correlations that have been found between reduced pressure transducer data and particle properties, the most encouraging (and least expected) are apparent correlations with pyrocarbon anisotropy. No conclusion can be drawn at this time as to whether the anisotropy is directly linked to the structure of the pressure fluctuations (e.g., mechanical impactation of the pyrocarbon surface) or indirectly associated via one or more process parameters that also influence the structure of the pressure fluctuations. Nonetheless, linear multivariate regressions are encouraging. Possible correlations are shown in Figure 28 and Figure 29 for the IPyC and OPyC diattenuation measurements. The form of the equations used for the correlations are shown in Equation 1 and Equation 2.

$$N_{IPyC} = N_o + a \cdot H_{1a, Mid} + b \cdot \sigma_{3, Mid} + c \cdot H_{2, End} + d \cdot (P_{inlet, End} - P_{inlet, Start}) \quad \text{Equation 1}$$

$$N_{OPyC} = N_o + a \cdot DP_{inlet, Start} + b \cdot \sigma_{3, Start} + c \cdot (P_{inlet, End} - P_{inlet, Start}) \quad \text{Equation 2}$$

where:

- $a, b, c, d$  = Regression coefficients
- $DP_{inlet}$  = Differential pressure across the gas distributor and bed during the layer deposition.
- $H_{1a}$  = Hurst exponent over the lag interval of 20 to 70 observations
- $H_2$  = Hurst exponent over the lag interval of 120 to 600 observations
- $N$  = Mean optical diattenuation of the pyrocarbon layer
- $N_o$  = Regressed intercept for optical diattenuation
- $P_{inlet}$  = Absolute pressure at the gas inlet
- $\sigma_3$  = Standard deviation of the Hurst exponent over the lag interval of 600 to 1,600 observations.

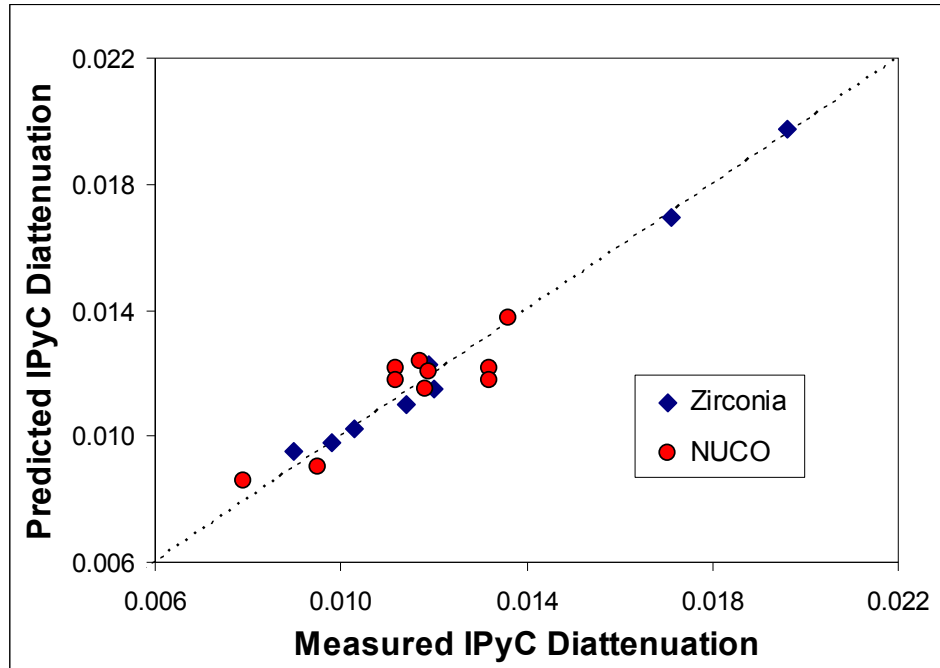


Figure 28. Comparison of IPyC diattenuation measurements with predicted values.

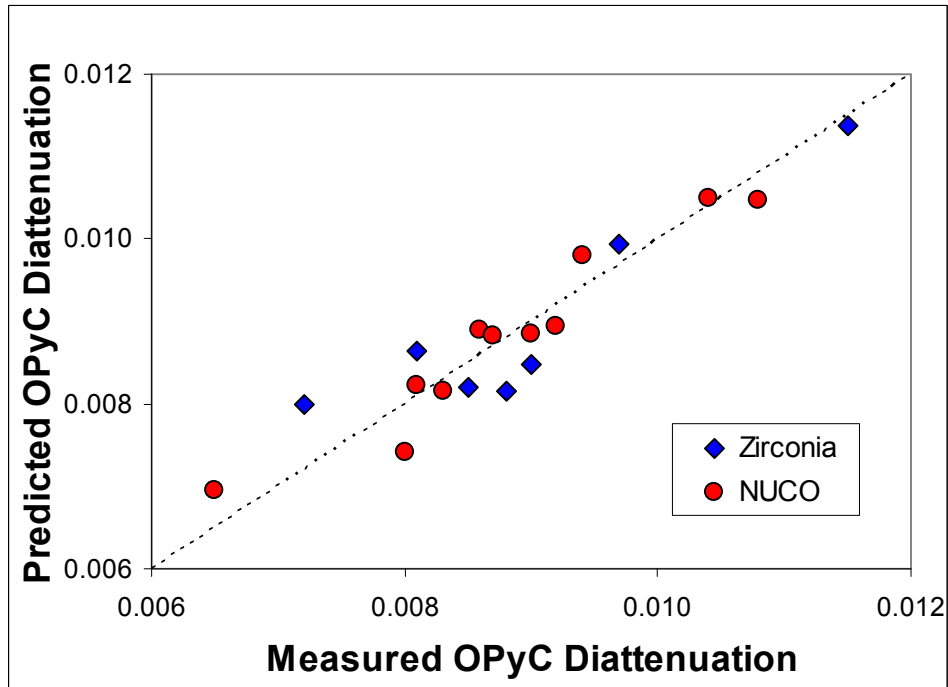


Figure 29. Comparison of OPyC diattenuation measurements with predicted values.

The diattenuation data were regressed separately for the coated zirconia surrogate and NUCO kernels because the coated surrogate does not fully reproduce the same fluid dynamics within the bed as coated NUCO particles in spite of having nearly identical particle diameters and densities. Two possible explanations have been identified that could explain the differences in the fluid dynamics, namely; rotational inertia and thermal diffusivity. The mass of the coated NUCO particles is more concentrated near the center than is the case for the coated zirconia, therefore a coated NUCO particle can change its angular velocity more readily. The zirconia kernels are larger in diameter and less dense than the NUCO kernels. A buffer layer of approximately half the normal thickness is applied to the zirconia kernel, which yields a particle having closely matched particle density and diameter relative to the coated NUCO. The buffer layer, being relatively thin, and the large zirconia kernel cannot be expected to have the same thermal properties as the buffer coated NUCO. Consequently, the rate of heat transfer from particles to the cold gas stream will likely differ, which impacts the shape, size, and gas composition of the bubbles.

The lack of full fluid dynamics similitude is illustrated by the correlations between the standard deviation of the Hurst exponent calculated for the (lag) range of 600–1,600 observations as shown in Figure 30. This standard deviation correlates well with the IPyC diattenuation for either the zirconia surrogate or the NUCO particles; however, the slopes of the regressed lines have slopes with opposite signs. Other similar incidents have been observed where regressed slopes for correlations between pressure fluctuation data and particle properties had opposite signs.

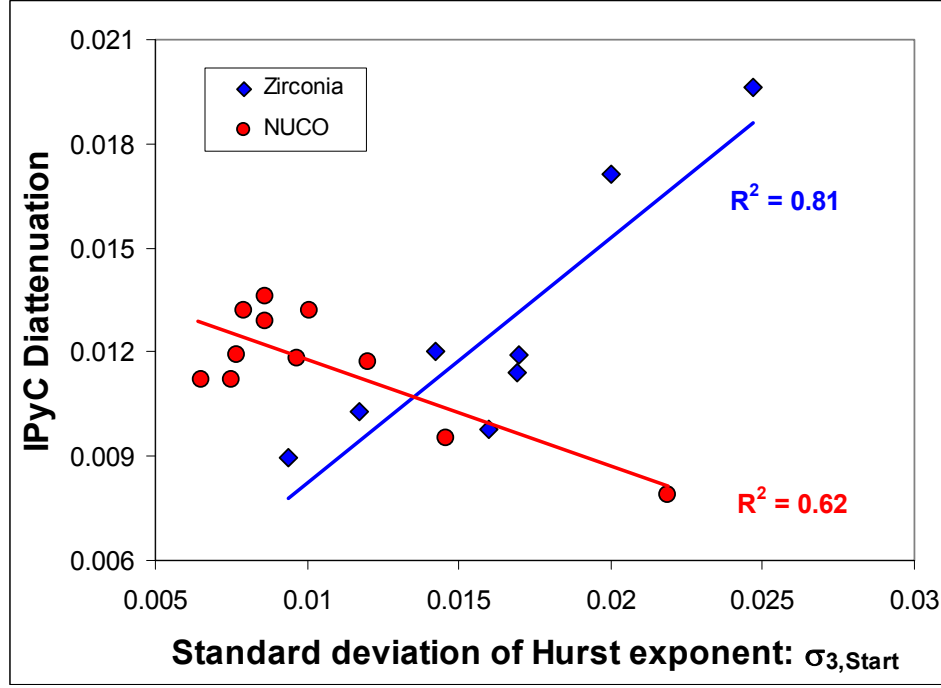


Figure 30. Illustration of apparent differences in the fluid dynamics for coated NUCO and zirconia surrogates.

The standard deviations of several Hurst exponents have been correlated with the final aspect ratio of the particles following OPyC deposition as expressed in Equation 3. As discussed above, the coefficients were regressed separately for the coated zirconia surrogates, the baseline NUCO particles, and the NUCO particles coated using the argon variant for the SiC layer. The predicted aspect ratios are shown in Figure 31.

$$AR_{OPyC} = AR_o + a \cdot \sigma_{3,Start} + b \cdot \sigma_{1a,End} + c \cdot \sigma_{1b,End} + d \cdot \sigma_{3,End} \quad \text{Equation 3}$$

where:

- $a, b, c, d$  = Regression coefficients
- $AR_o$  = Regressed intercept for the aspect ratio
- $AR_{OPyC}$  = Aspect ratio of particle following OPyC deposition
- $P_{inlet}$  = Absolute pressure at the gas inlet
- $\sigma_{1a}$  = Standard deviation of the Hurst exponent over the lag interval of 3 to 20 observations
- $\sigma_{1b}$  = Standard deviation of the Hurst exponent over the lag interval of 20 to 70 observations
- $\sigma_3$  = Standard deviation of the Hurst exponent over the lag interval of 600 to 1,600 observations.

Some apparent correlations between the various values derived from the pressure fluctuation data and particle properties may be falsely indicated because of relatively limited data. Regressed coefficients will likely evolve or dissolve as more data become available. This is inherent to the investigation of new techniques and methods for analyzing processes.

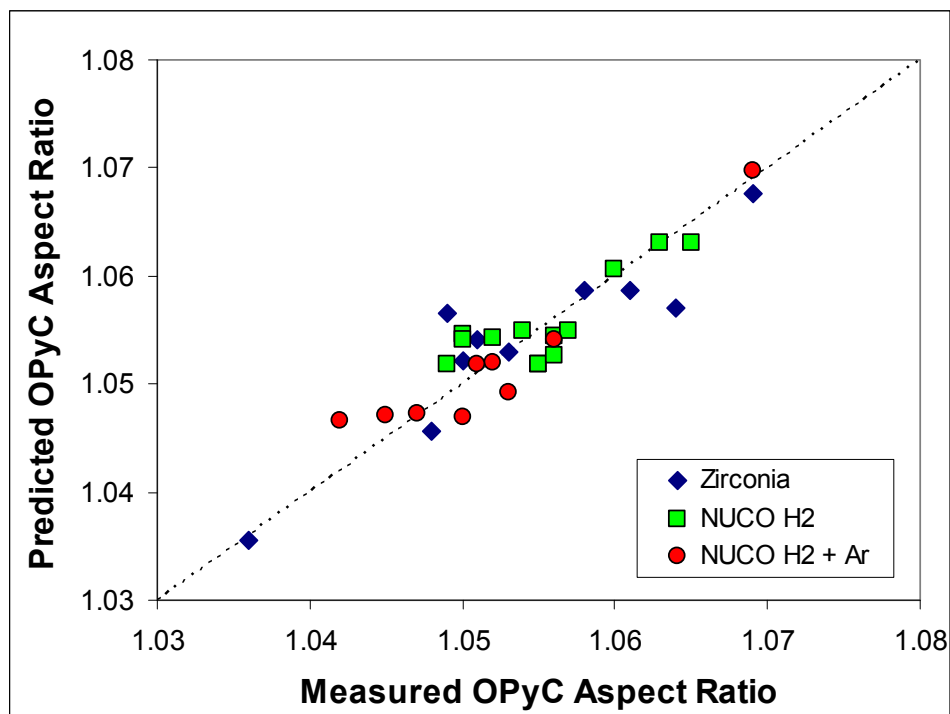


Figure 31. Comparison of predicted to measured OPyC aspect ratios.

Analysis of the structure in the gas inlet pressure fluctuations have been helpful in identifying what appears to be desirable fluidizing conditions in the bed during the depositions of the coatings. Promising correlations have been found between particle properties and values derived from the pressure fluctuations. One of the most encouraging possibilities is the ability to predict the anisotropy of the pyrocarbon layers, as this could lead to an early confirmation that process parameters were as indicated (no significant thermocouple drift) and a potential reduction in the requirement to analyze the anisotropy of each coater batch.



## 8. TABLING YIELD AND KERNEL CHARGE SIZE

Particles batches unloaded from the coater are sieved to remove undersize and oversize particles and then tabled to remove less spherical particles. The table separates the batch into three fractions or bins. Current practice is to use only particles from one bin, Bin #3, as product. No work was done this year to improve yield. As shown in Figure 32, yields from the tabling operation have ranged from a low of 47% to a high of 90%. Causes for the variability in yield from batch to batch have not been determined.

A study is being planned to optimize product yield. Initial efforts would analyze particles from Bin #2 to determine if they meet SiC defect fraction and aspect ratio specifications and, hence, could be included in the product. If these particles as a whole do not meet specifications, adjusting tabling parameters or retabling Bin 2 particles should be considered.

The SiC defect fraction specification for AGR-2 particles was not changed from that for AGR-1 particles, but the intention of the AGR program is to reduce the SiC defect fraction for future test particles. Thus, the yield improvement studies should also be constrained by a SiC defect fraction specification of  $2.5 \times 10^{-5}$ , rather than the AGR-2 specification of  $1 \times 10^{-4}$ .

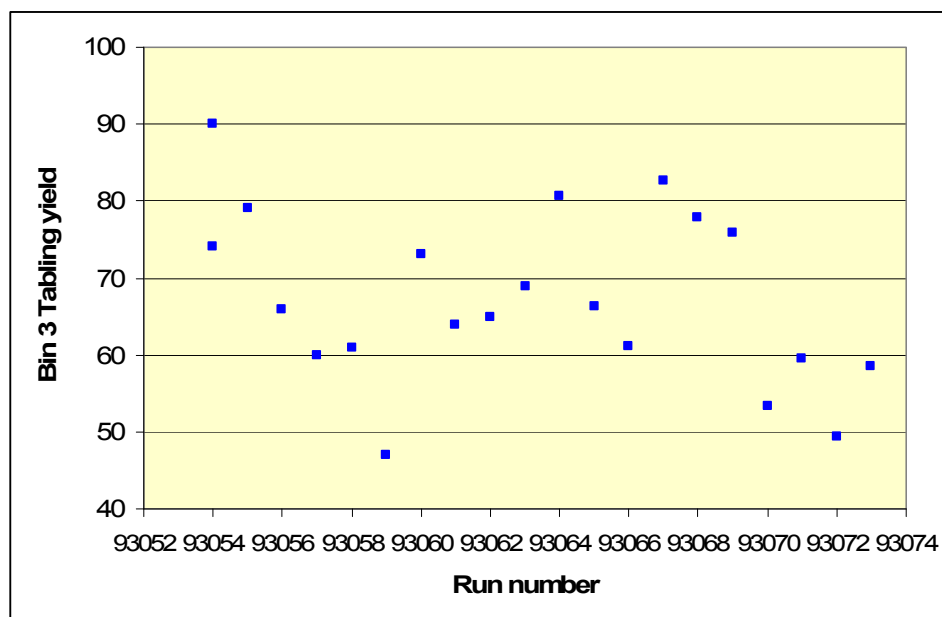


Figure 32. Product yields in tabling batches 93053 through 93074.

The kernel charge size also needs to be optimized to improve the economics of coating. A charge size of 1.5 kg of kernels was used for all tests until run 93046. The charge for run 93046 was dropped to 1.275 kg and improvements in pyrocarbon anisotropy and particle sphericity were seen. Based on results for this one run, a charge size of 1.3 kg was used for later tests and for AGR-2 particle production runs, but data from these later runs do not confirm the advantages of the lower charge seen in run 93046. Tests are planned to determine the upper practicable limit of charge size for the B&W coater.

## **9. COATING AGR-2 UCO PARTICLES**

Four runs were made to coat LEU UCO kernels from July 28 to August 7, 2008. Target flow rates, coating temperature, and coating times were the same for all runs for the buffer, IPyC, and OPyC layers. The first two runs used baseline conditions for the SiC layer, and the second two used variant conditions. Hot samples of IPyC particles were taken in the first and third runs, and hot samples of buffer particles in the second and fourth runs. Two additional runs using baseline conditions were performed later to provide additional particles for possible use either for AGR-2 fuel or as driver particles for AGR-3 & 4 fuel. Once characterization of all AGR-2 particle batches is complete, one batch of each of the baseline and variant runs will be selected for use as AGR-2 fuel.

## 10. CONCLUSIONS, RECOMMENDATIONS AND PLANS

The coater tests performed by B&W in FY 2008 led to successful identification of process parameters for the B&W 6-inch-diameter coater to produce AGR-2 UCO particles. Data were obtained that provided a basis for selecting coating conditions for AGR-2 baseline and variant particles, and these conditions were used in a series of 11 qualification tests followed by AGR-2 production runs. Pressure data was collected in each test and has been used to develop several promising correlations with coated particle properties.

Improvements need to be made in the coating process to be economically viable for a fuel fabrication facility, to improve the reliability of meeting specifications, and to prepare for the reduced defect fraction specification for AGR-5 & 6 particles. To achieve the desired improvements the coating development program will focus on the following actions in the coming years as funding allows:

- Reinsert the internal thermocouple into the coater to measure bed temperatures during the coater tests in FY 2009 and to determine whether its presence has an effect on SiC defects.
- Perform tests to determine the maximum kernel charge size that can be coated in B&W's 6-inch coater while reliably meeting product specifications. These tests could include tests with increased coating gas fractions for pyrocarbon layers.
- Evaluate modifications to off-gas handling and furnace exhaust equipment to enable higher coating gas flow rates. This study is needed as a prerequisite to maximizing charge size.
- Improve control of the MTS rate by replacing the current MTS feed system with direct liquid injection/total vaporization system.
- Review and improve the design of the hot sampler to reduce the risk of losing the sample cup during a coating run, to increase the capacity of the sampler, and to enable taking both buffer and IPyC samples during the same coating run. Less brittle materials (compared to molybdenum) should be considered for the wire from which the cup is hung.
- Perform coater tests to further optimize argon and MTS concentrations and coating temperature for SiC coating by:
  - Testing variant conditions for coating UO<sub>2</sub> kernels
  - Reducing total coating time by increasing MTS rates
  - Better defining the acceptable operating region of MTS concentration and gas flow rates that result in acceptable SiC layer properties.
- Further evaluate the impacts of increasing the SiC coating thickness specification. This would first involve fuel performance modeling studies and then possibly particle or SiC layer crush strength tests and coater tests.
- Perform upgrading studies to improve the particle yield. These studies would begin with characterizing currently rejected particle fractions and could lead to changes in upgrading methods or upgrading equipment.
- Perform additional particle characterization to seek to identify causes of SiC defects and possibly, based on the results of upgrading studies, additional tests to consistently achieve defect fractions below the expected AGR-5 & -6 specification limit.
- Perform coater tests with alternative chalice and nozzle designs as ways to achieve reduced defect fractions and more consistent batch-to-batch particle properties.
- Evaluate alternative methods of measuring bed temperature or means of detecting thermocouple drift.

- Acquire and install an ellipsometer at B&W for determining pyrocarbon diattenuation.
- Perform tests to better determine the dependence of buffer density on coating temperature, gas flow rates and coating gas fraction, and the causes of density variations in runs in which no parameters are deliberately varied.
- Investigate annulus/primary gas ratios to improve particle be circulation by analyzing pressure fluctuation data.
- Resolve discrepancies in OPyC surface connected porosity measurements between B&W and ORNL.
- Investigate possible designs for bottom unloading of the coater.

## 11. REFERENCES

1. D. Petti, R. Hobbins, J. Kendall, J. Saurwein, *Technical Program Plan for the Advanced Gas Reactor Fuel Development and Qualification Program*, INL/EXT-05-00465, Revision 1, August, 2005.
2. C. M. Barnes, D. W. Marshall, "Advanced Gas Reactor Coater Scale Up Plan," PLN-1975, Revision 0, February 1, 2006.
3. D. W. Marshall, "Six-Inch TRISO Fuel Coater Design for AGR-2," EDF-6666, Revision 1, September 14, 2006.
4. D. W. Marshall, C. M. Barnes, *AGR Fuel Development – Coater and Control System Upgrade*, INL/EXT-07-12458, March 2007.
5. C. M. Barnes, D. W. Marshall, *FY 2007 Six-inch Diameter Coater Test Report*, INL/EXT-07-13090, September, 2007.
6. C. M. Barnes, "AGR-2 Fuel Specification," SPC-923, Rev. 1, April 30, 2008.
7. L. H. Ford, N. S. Hibbert, D. G. Martin, "Recent Developments of Coatings for GCFR and HTGCR Particles and Their Performance," *J. Nuclear Materials* 45, 1972-3, pp. 139-149.
8. F. Charollais, S. Fonquernie, C. Perrais, M. Perez, O. Dugne, F. Cellier, G. Harbonnier, M.-P. Vitali, CEA and AREVA R&D on HTR Fuel Fabrication and Presentation of the CAPRI Experimental Manufacturing Line, *Nuclear Engineering and Design* 236 (5-6), March 2006, pp. 534-542.
9. H. Beutler, R. L. Beatty, J. H. Coobs, "Low-Density Pyrolytic-Carbon Coating for Nuclear Fuel Particles," *Electrochemical Technology* 5, 1967, pp. 189-194.
10. R. A. Lowden, J. D. Hunn, S. D. Nunn, A. K. Kercher, J. R. Price, P. A. Menchhofer, G. E. Jellison, Jr., *Effects of Deposition Conditions on the Properties of Pyrolytic Carbon Deposited in a Fluidized Bed*, ORNL/TM-2005/533, September 2005.
11. K. Minato and K. Fukuda, "Chemical Vapor Deposition of Silicon Carbide for Coated Fuel Particles," *J. of Nuclear Materials* 149, 1987, pp. 233-246.
12. R. A. Lowden, "Fabrication of Baseline and Variant Particle Fuel for AGR-1," ORNL/CF-06/02, Rev. 0, April 2006.
13. R. E. Bullock, "Historical Review of Coated-Particle Fuel as Related to the Performance of TRISO-P Particles," CEGB-M-93-1274 Oct 23, 1993
14. D. S. Boyalakuntla, S. Pannala C. E. A. Finney, C. S. Daw, "ORNL FY05 Process Modeling Summary Report for the Advanced Gas Reactor Fuel Development and Qualification Program: Hydrodynamics, Heat and Mass Transfer," ORNL/CF-05/13, August 2005.



## **Appendix A**

### **Coater Run Data**





## Appendix A—Coater Run Data

Table A-1. Coating parameter and particle properties for runs 93033-93035.

	Run ID		
	93033	93034	93035
<b>Kernels</b>			
Charge size, kg	1.5	1.5	1.5
Mean diameter, microns	530	530	530
Type	YSZ	YSZ	YSZ
<b>Buffer</b>			
Control Temp, °C	1474	1474	1473
Bed TC Temp, start, °C	1388	1468	1373
Bed TC Temp, end, °C	1566	1556	1510
Acetylene, slpm	99.1	99.5	99
Argon, slpm	55.9	56	55
Annular argon, slpm	30	30	30
Total gas flow, slpm	185.1	185.6	184
Coating gas fraction	0.54	0.54	0.54
Coating time, minutes	3.5	3.5	3.5
Coating rate, $\mu\text{m}/\text{min}$	14.29	13.71	13.86
Buffer thickness, $\mu\text{m}$	50	48	48.5
Buffer density, $\text{g}/\text{cm}^3$	Not measured	Not measured	Not measured
<b>IPyC</b>			
Control Temp, °C	1338	1338	1338
Bed TC Temp, start, °C	1265	1284	1271
Bed TC Temp, end, °C	1268	1282	1268
Acetylene, slpm	30	40.2	41
Propylene, slpm	26	34	34
Argon, slpm	112	96	96
Annular argon, slpm	20	17.2	17.2
Total gas flow, slpm	188	187.4	188.2
Coating gas fraction	0.30	0.40	0.40
Coating gas ratio	0.87	0.85	0.83
Coating time, minutes	15	11.25	10.25
Coating rate, $\mu\text{m}/\text{min}$	3.47	4.36	4.42
IPyC thickness, $\mu\text{m}$	52	49	45.3
IPyC density, $\text{g}/\text{cm}^3$	Not measured	1.874	1.905
IPyC BAF <sub>o</sub>	1.0309	Not measured	1.0357
IPyC porosity, $\text{ml}/\text{m}^2$	Not measured	Not measured	Not measured
<b>SiC</b>			
Control Temp, °C	1600	1600	1600
Bed TC Temp, start, °C	1429	1500	1436
Bed TC Temp, end, °C	1416	1492	1455
MTS flow, $\text{g}/\text{hr}$	905	896	901

Table A-1. (continued).

	Run ID		
	93033	93034	93035
H <sub>2</sub> flow, MTS sweep, slpm	25	25	25
H <sub>2</sub> flow, slpm	143.5	143	143.3
Annular H <sub>2</sub> flow, slpm	25.2	25.2	25.2
Argon, slpm	0	0	0
Total gas flow, slpm	193.7	193.2	193.5
Ar, mol %	0	0	0
Mole % MTS	1.25%	1.15%	1.15%
Coating time, minutes	120	47	140
Coating rate, $\mu\text{m}/\text{min}$	0.15	0.17	0.15
SiC thickness, $\mu\text{m}$	18	8	20.9
SiC density, $\text{g}/\text{cm}^3$	3.201	3.186	Not measured
SiC aspect ratio	1.032	Not measured	Not measured
SiC defects	NA	NA	NA
SiC defect sample size	NA	NA	NA
<b>OPyC</b>			
Control Temp, °C	NA	1354	1353
Bed TC Temp, start, °C	NA	1286	1291
Bed TC Temp, end, °C	NA	1288	1290
Acetylene, slpm	NA	36.2	36.4
Propylene, slpm	NA	30.7	30.8
Argon, slpm	NA	100	100
Annular argon, slpm	NA	45	45
Total gas flow, slpm	NA	211.9	212.2
Coating gas fraction	NA	0.32	0.32
Coating gas ratio	NA	0.85	0.85
Coating time, minutes	NA	15	15
Coating rate, $\mu\text{m}/\text{min}$	NA	2.67	2.72
OPyC thickness, $\mu\text{m}$	NA	40	40.8
OPyC density, $\text{g}/\text{cm}^3$	NA	1.875	1.892
OPyC BAF <sub>o</sub>	NA	Not measured	1.0264
OPyC porosity, $\text{ml}/\text{m}^2$	NA	Not measured	0.9
OPyC aspect ratio	NA	1.048	1.051
Missing OPyC	NA	1/1096	0/978
<b>Other/notes</b>			
93033 Run terminated when bed stuck during SiC due to melting of kernel load tube			
93034 Bed stuck during SiC coating, refluidized with Ar and OPyC applied			

Table A-2. Coating parameter and particle properties for runs 93044-93047.

Run ID				
	93044	93045	93046	93047
<b>Kernels</b>				
Charge size, kg	1.5	1.5	1.275	1.5
Mean diameter, microns	530	530	530	530
Type	YSZ	YSZ	YSZ	YSZ
<b>Buffer</b>				
Control Temp, °C	1473	1474	1473	1474
Bed TC Temp, start, °C	1378	1354	1365	1378
Bed TC Temp, end, °C	1527	1548	1551	1513
Acetylene, slpm	99.4	99.8	100	99
Argon, slpm	55	55	55	55
Annular argon, slpm	30	30	30	30
Total gas flow, slpm	184.4	184.8	185	184
Coating gas fraction	0.54	0.54	0.54	0.54
Coating time, minutes	3.5	3.5	2.9	3.5
Coating rate, $\mu\text{m}/\text{min}$	13.77	14.29	20.21	15.23
Buffer thickness, $\mu\text{m}$	48.2	50	58.6	53.3
Buffer density, $\text{g}/\text{cm}^3$	Not measured	Not measured	Not measured	Not measured
<b>IPyC</b>				
Control Temp, °C	1339	1337	1339	1339
Bed TC Temp, start, °C	1240	1300	1281	1299
Bed TC Temp, end, °C	1237	1299	1270	1301
Acetylene, slpm	30.5	34.6	30.4	30
Propylene, slpm	25.7	29.1	25.5	25
Argon, slpm	113	127.7	113	113
Annular argon, slpm	20	22.9	20.1	20
Total gas flow, slpm	189.2	214.3	189	188
Coating gas fraction	0.30	0.30	0.30	0.29
Coating gas ratio	0.84	0.84	0.84	0.83
Coating time, minutes	12	10.5	9.8	12
Coating rate, $\mu\text{m}/\text{min}$	3.28	3.50	4.17	3.28
IPyC thickness, $\mu\text{m}$	39.4	36.7	40.9	39.3
IPyC density, $\text{g}/\text{cm}^3$	1.887	1.887	1.888	1.862
IPyC BAF <sub>o</sub>	1.036	1.0342	1.0269/1.0306	1.0294
IPyC porosity, $\text{ml}/\text{m}^2$	1.8	2.1	Not measured	2.3
<b>SiC</b>				
Control Temp, °C	1600	1600	1600	1600
Bed TC Temp, start, °C	1469	1469	1436	1498
Bed TC Temp, end, °C	1458	1402	1422	1500

Table A-2. (continued).

Run ID				
	93044	93045	93046	93047
MTS flow, g/hr	1142	1135	1137	1757
H <sub>2</sub> flow, MTS sweep, slpm	40	40	40	49
H <sub>2</sub> flow, slpm	128.3	128.3	128.4	120
Annular H <sub>2</sub> flow, slpm	25.2	25.2	25.2	25.2
Argon, slpm	0	0	0	0
Total gas flow, slpm	193.5	193.5	193.6	194.2
Ar, mol %	0	0	0	0
Mole % MTS	1.45%	1.44%	1.44%	2.25%
Coating time, minutes	140	140	114	90
Coating rate, $\mu\text{m}/\text{min}$	0.26	0.24	0.29	0.36
SiC thickness, $\mu\text{m}$	36.3	34.1	33	32.4
SiC density, $\text{g}/\text{cm}^3$	3.198	3.201	3.197	3.193
SiC aspect ratio	Not measured	Not measured	Not measured	Not measured
SiC defects	Not measured	Not measured	Not measured	Not measured
SiC defect sample size	NA	NA	NA	NA
<b>OPyC</b>				
Control Temp, $^{\circ}\text{C}$	1353	1351	1353	1353
Bed TC Temp, start, $^{\circ}\text{C}$	1280	1270	1280	1313
Bed TC Temp, end, $^{\circ}\text{C}$	1277	1208	1260	1331
Acetylene, slpm	36.5	45.6	37.3	36.3
Propylene, slpm	30.8	38.5	30.7	30.7
Argon, slpm	100	87.7	100	100
Annular argon, slpm	45	39.5	45	45
Total gas flow, slpm	212.3	211.3	213	212
Coating gas fraction	0.32	0.40	0.32	0.32
Coating gas ratio	0.84	0.84	0.82	0.85
Coating time, minutes	15	11.75	12.3	15
Coating rate, $\mu\text{m}/\text{min}$	2.72	3.34	3.20	2.98
OPyC thickness, $\mu\text{m}$	40.8	39.3	39.4	44.7
OPyC density, $\text{g}/\text{cm}^3$	1.891	1.912	1.898	1.833
OPyC BAF <sub>o</sub>	1.027	1.0255	1.0243/1.0249	1.0216
OPyC porosity, $\text{ml}/\text{m}^2$	1	1.2	1	1.4
OPyC aspect ratio	1.053	1.05	1.036	1.049
Missing OPyC	Not measured	Not measured	Not measured	Not measured
<b>Other/notes</b>			BAF <sub>o</sub> measured on 2 separate samples	

Table A-3. Coating parameter and particle properties for runs 93048-93051.

	Run ID			
	93048	93049	93050	93051
<b>Kernels</b>				
Charge size, kg	1.5	1.5	1.275	1.5
Mean diameter, microns	429	429	429	429
Type	NUCO	NUCO	NUCO	NUCO
<b>Buffer</b>				
Control Temp, °C	1474	1474	1475	1477
Bed TC Temp, start, °C	NA	NA	NA	NA
Bed TC Temp, end, °C	NA	NA	NA	NA
Acetylene, slpm	88	88	99.6	99.5
Argon, slpm	49	49	55	55.3
Annular argon, slpm	26	26	30	30.1
Total gas flow, slpm	163	163	184.6	184.9
Coating gas fraction	0.54	0.54	0.54	0.54
Coating time, minutes	6.7	6.7	5.8	5.8
Coating rate, $\mu\text{m}/\text{min}$	15.84	17.01	22.10	NA
Buffer thickness, $\mu\text{m}$	106.1	114	128.2	Not measured
Buffer density, $\text{g}/\text{cm}^3$	1.1	Not measured	Not measured	Not measured
<b>IPyC</b>				
Control Temp, °C	1338	1339	1339	1339
Bed TC Temp, start, °C	NA	NA	NA	NA
Bed TC Temp, end, °C	NA	NA	NA	NA
Acetylene, slpm	30.3	30.5	30.3	30.4
Propylene, slpm	25.5	25.5	25.6	25.6
Argon, slpm	113	113	113	113
Annular argon, slpm	20	20	20	20
Total gas flow, slpm	188.8	189	188.9	189
Coating gas fraction	0.30	0.30	0.30	0.30
Coating gas ratio	0.84	0.84	0.84	0.84
Coating time, minutes	12	12	9.8	12
Coating rate, $\mu\text{m}/\text{min}$	3.38	3.17	3.58	NA
IPyC thickness, $\mu\text{m}$	40.5	38	35.1	Not measured
IPyC density, $\text{g}/\text{cm}^3$	Not measured	1.817	1.826	1.781
IPyC BAF <sub>o</sub>	1.0285	1.0238	Not measured	Not measured
IPyC porosity, $\text{ml}/\text{m}^2$	Not measured	1.9	2.7	2.6
<b>SiC</b>				
Control Temp, °C	1600	1599	1599	1599
Bed TC Temp, start, °C	NA	NA	NA	NA
Bed TC Temp, end, °C	NA	NA	NA	NA

Table A-3. (continued).

	Run ID			
	93048	93049	93050	93051
MTS flow, g/hr	1261	1300	1337	1822
H <sub>2</sub> flow, MTS sweep, slpm	40	40	40	40
H <sub>2</sub> flow, slpm	128.3	128	128.5	128.6
Annular H <sub>2</sub> flow, slpm	25.3	25	25.4	25.5
Argon, slpm	0	0	0	0
Total gas flow, slpm	193.6	193	193.9	194.1
Ar, mol %	0	0	0	0
Mole % MTS	1.60%	1.65%	1.69%	2.27%
Coating time, minutes	140	140	114	30
Coating rate, $\mu\text{m}/\text{min}$	0.25	0.25	0.30	NA
SiC thickness, $\mu\text{m}$	34.7	34.8	33.7	Not measured
SiC density, $\text{g}/\text{cm}^3$	3.2	3.197	3.196	Not measured
SiC aspect ratio	Not measured	1.038	1.038	Not measured
SiC defects	0.3	1	66	Not measured
SiC defect sample size	50,000	50,000	50,000	NA
<b>OPyC</b>				
Control Temp, °C	1352	1352	1352	1352
Bed TC Temp, start, °C	NA	NA	NA	NA
Bed TC Temp, end, °C	NA	NA	NA	NA
Acetylene, slpm	36.4	36.6	36.6	36.5
Propylene, slpm	30.8	31	30.9	30.9
Argon, slpm	100	100	100	100
Annular argon, slpm	45	45	45	45
Total gas flow, slpm	212.2	212.6	212.5	212.4
Coating gas fraction	0.32	0.32	0.32	0.32
Coating gas ratio	0.85	0.85	0.84	0.85
Coating time, minutes	15	15	12.3	15
Coating rate, $\mu\text{m}/\text{min}$	2.83	2.81	3.33	2.82
OPyC thickness, $\mu\text{m}$	42.5	42.2	41	42.3
OPyC density, $\text{g}/\text{cm}^3$	1.835	1.818	1.82	1.8
OPyC BAF <sub>o</sub>	1.0252	1.0196	Not measured	Not measured
OPyC porosity, $\text{ml}/\text{m}^2$	1.1	0.9	<0.5	0.6
OPyC aspect ratio	1.063	1.06	1.053	1.056
Missing OPyC	0/898	0/840	0/785	NA
<b>Other/notes</b>				Run aborted 30 min into SiC due to liquid level alarm in scrub system

Table A-4. Coating parameter and particle properties for runs 93052-93055.

Run ID				
	93052	93053	93054	93055
<b>Kernels</b>				
Charge size, kg	1.5	1.5	1.3	1.3
Mean diameter, microns	429	429	429	429
Type	NUCO	NUCO	NUCO	NUCO
<b>Buffer</b>				
Control Temp, °C	1476	1473	1473	1474
Bed TC Temp, start, °C	NA	NA	NA	NA
Bed TC Temp, end, °C	NA	NA	NA	NA
Acetylene, slpm	87.7	88.1	92.8	97.7
Argon, slpm	49.1	49.1	43.5	39
Annular argon, slpm	26	26.1	18.9	26
Total gas flow, slpm	162.8	163.3	155.2	162.7
Coating gas fraction	0.54	0.54	0.60	0.60
Coating time, minutes	6.7	6.7	5.4	5.2
Coating rate, $\mu\text{m}/\text{min}$	17.30	16.57	21.85	21.56
Buffer thickness, $\mu\text{m}$	115.9	111	118	112.1
Buffer density, $\text{g}/\text{cm}^3$	Not measured	Not measured	Not measured	1.09
<b>IPyC</b>				
Control Temp, °C	1339	1338	1339	1339
Bed TC Temp, start, °C	NA	NA	NA	NA
Bed TC Temp, end, °C	NA	NA	NA	NA
Acetylene, slpm	30.2	30.4	30.1	30.2
Propylene, slpm	25.5	25.5	25.2	25.5
Argon, slpm	113	113	112.3	112
Annular argon, slpm	20.1	20	19.9	19.9
Total gas flow, slpm	188.8	188.9	187.5	187.6
Coating gas fraction	0.30	0.30	0.29	0.30
Coating gas ratio	0.84	0.84	0.84	0.84
Coating time, minutes	12	12	10.5	10.5
Coating rate, $\mu\text{m}/\text{min}$	3.48	3.56	3.40	3.47
IPyC thickness, $\mu\text{m}$	41.7	42.7	35.7	36.4
IPyC density, $\text{g}/\text{cm}^3$	1.789	1.819	Not measured	Not measured
IPyC BAF <sub>o</sub>	Not measured	Not measured	1.0351	1.0408
IPyC porosity, $\text{ml}/\text{m}^2$	2.7	2.3	Not measured	Not measured
<b>SiC</b>				
Control Temp, °C	1550	1348	1599	1551
Bed TC Temp, start, °C	NA	NA	NA	NA
Bed TC Temp, end, °C	NA	NA	NA	NA

Table A-4. (continued).

	Run ID			
	93052	93053	93054	93055
MTS flow, g/hr	1704	1723	2084	1645
H <sub>2</sub> flow, MTS sweep, slpm	49	49	49	40
H <sub>2</sub> flow, slpm	45.9	25.1	113.8	47.5
Annular H <sub>2</sub> flow, slpm	19.5	19.5	25.7	18.2
Argon, slpm	28.7	49.3	0	26.5
Total gas flow, slpm	143.1	142.9	188.5	132.2
Ar, mol %	20.1%	34.5%	0	20.0%
Mole % MTS	2.90%	2.90%	2.68%	3.01%
Coating time, minutes	90	90	65.7	100
Coating rate, $\mu\text{m}/\text{min}$	0.35	0.29	0.31	0.37
SiC thickness, $\mu\text{m}$	31.3	25.8	27.8	37.2
SiC density, $\text{g}/\text{cm}^3$	3.217	3.145	3.185	3.197
SiC aspect ratio	1.04	1.044	1.035	1.037
SiC defects	15	16	15	1
SiC defect sample size	50,000	50,000	50,000	50,000
<b>OPyC</b>				
Control Temp, °C	1352	1353	1352	1351
Bed TC Temp, start, °C	NA	NA	NA	NA
Bed TC Temp, end, °C	NA	NA	NA	NA
Acetylene, slpm	36.5	36.5	36.3	36.6
Propylene, slpm	30.9	30.7	31	31.5
Argon, slpm	100	100	102.1	102
Annular argon, slpm	45	45	47	46
Total gas flow, slpm	212.4	212.2	216.4	216.1
Coating gas fraction	0.32	0.32	0.31	0.32
Coating gas ratio	0.85	0.84	0.85	0.86
Coating time, minutes	15	15	12.9	12.9
Coating rate, $\mu\text{m}/\text{min}$	2.82	3.23	3.13	3.09
OPyC thickness, $\mu\text{m}$	42.3	48.4	40.4	39.8
OPyC density, $\text{g}/\text{cm}^3$	1.8	1.798	1.904	1.937
OPyC BAF <sub>o</sub>	Not measured	Not measured	1.025	1.0325
OPyC porosity, $\text{ml}/\text{m}^2$	0.6	1.4	0.8	0.6
OPyC aspect ratio	1.056	1.069	1.056	1.055
Missing OPyC	0/844	0/825	0/884	0/777
<b>Other/notes</b>				
			TC-7 replaced after run 93054	



Table A-5. Coating parameter and particle properties for runs 93056-93058.

	Run ID		
	93056	93057	93058
<b>Kernels</b>			
Charge size, kg	1.3	1.3	1.3
Mean diameter, microns	429	429	429
Type	NUCO	NUCO	NUCO
<b>Buffer</b>			
Control Temp, °C	1473	1473	1474
Bed TC Temp, start, °C	NA	NA	NA
Bed TC Temp, end, °C	NA	NA	NA
Acetylene, slpm	97.5	93.1	93
Argon, slpm	39	43.6	43.6
Annular argon, slpm	26	18.9	18.8
Total gas flow, slpm	162.5	155.6	155.4
Coating gas fraction	0.60	0.60	0.60
Coating time, minutes	5.2	4.6	4.6
Coating rate, $\mu\text{m}/\text{min}$	22.58	22.33	23.37
Buffer thickness, $\mu\text{m}$	117.4	102.7	107.5
Buffer density, $\text{g}/\text{cm}^3$	1.06	Not measured	1.07
<b>IPyC</b>			
Control Temp, °C	1339	1339	1339
Bed TC Temp, start, °C	NA	NA	NA
Bed TC Temp, end, °C	NA	NA	NA
Acetylene, slpm	30.1	30.3	30
Propylene, slpm	25.5	25.5	25.5
Argon, slpm	112	112.2	112.4
Annular argon, slpm	19.8	19.9	19.8
Total gas flow, slpm	187.4	187.9	187.7
Coating gas fraction	0.30	0.30	0.30
Coating gas ratio	0.85	0.84	0.85
Coating time, minutes	10.5	11.8	11.8
Coating rate, $\mu\text{m}/\text{min}$	3.18	3.55	3.52
IPyC thickness, $\mu\text{m}$	33.4	41.9	41.5
IPyC density, $\text{g}/\text{cm}^3$	1.854	Not measured	1.913
IPyC BAF <sub>o</sub>	1.0358	Not measured	Not measured
IPyC porosity, $\text{ml}/\text{m}^2$	2.3	Not measured	1.9
<b>SiC</b>			
Control Temp, °C	1550	1599	1600
Bed TC Temp, start, °C	NA	NA	NA
Bed TC Temp, end, °C	NA	NA	NA

Table A-5. (continued).

	Run ID		
	93056	93057	93058
MTS flow, g/hr	1520	1904	1217
H <sub>2</sub> flow, MTS sweep, slpm	40	49	40
H <sub>2</sub> flow, slpm	28.4	119.6	122
Annular H <sub>2</sub> flow, slpm	16.8	25.2	27
Argon, slpm	36.8	0	0
Total gas flow, slpm	122	193.8	189
Ar, mol %	30.2%	0	0
Mole % MTS	3.01%	2.39%	1.59%
Coating time, minutes	110	97	118
Coating rate, $\mu\text{m}/\text{min}$	0.36	0.47	0.28
SiC thickness, $\mu\text{m}$	39.5	45.2	33.3
SiC density, $\text{g}/\text{cm}^3$	3.201	3.194	3.202
SiC aspect ratio	1.036	1.036	1.039
SiC defects	<1	<1	8.5
SiC defect sample size	50,000	50,000	50,000
<b>OPyC</b>			
Control Temp, °C	1353	1352	1353
Bed TC Temp, start, °C	NA	NA	NA
Bed TC Temp, end, °C	NA	NA	NA
Acetylene, slpm	37	36.6	36.7
Propylene, slpm	31	31.1	31
Argon, slpm	102	102.1	102.1
Annular argon, slpm	45.9	45.9	45.9
Total gas flow, slpm	215.9	215.7	215.7
Coating gas fraction	0.31	0.31	0.31
Coating gas ratio	0.84	0.85	0.84
Coating time, minutes	12.9	12.9	12.9
Coating rate, $\mu\text{m}/\text{min}$	2.79	2.92	3.09
OPyC thickness, $\mu\text{m}$	36	37.7	39.9
OPyC density, $\text{g}/\text{cm}^3$	1.927	1.858	1.928
OPyC BAF <sub>o</sub>	1.0311	Not measured	Not measured
OPyC porosity, $\text{ml}/\text{m}^2$	0.4	0.7	Not measured
OPyC aspect ratio	1.051	1.052	1.055
Missing OPyC	0/809	0/809	0/865
<b>Other/notes</b>			2 analyses performed for SiC defects with equivalent results

Table A-6. Coating parameter and particle properties for runs 93059-93062.

Run ID				
	93059	93060	93061	93062
<b>Kernels</b>				
Charge size, kg	1.3	1.3	1.3	1.3
Mean diameter, microns	429	429	432	432
Type	NUCO	NUCO	NUCO	NUCO
<b>Buffer</b>				
Control Temp, °C	1475	1473	1474	1474
Bed TC Temp, start, °C	NA	NA	NA	NA
Bed TC Temp, end, °C	NA	NA	NA	NA
Acetylene, slpm	97.5	97.5	97.4	97.5
Argon, slpm	39.1	39.1	39	39
Annular argon, slpm	26.1	26	26	26
Total gas flow, slpm	162.7	162.6	162.4	162.5
Coating gas fraction	0.60	0.60	0.60	0.60
Coating time, minutes	4.6	4.6	4.1	4.1
Coating rate, $\mu\text{m}/\text{min}$	24.07	24.78	23.15	23.71
Buffer thickness, $\mu\text{m}$	110.7	114	94.9	97.2
Buffer density, $\text{g}/\text{cm}^3$	Not measured	Not measured	1.03	0.94
<b>IPyC</b>				
Control Temp, °C	1329	1329	1329	1329
Bed TC Temp, start, °C	NA	NA	NA	NA
Bed TC Temp, end, °C	NA	NA	NA	NA
Acetylene, slpm	30	30.3	30.5	30
Propylene, slpm	25.5	25.5	25.5	25.7
Argon, slpm	112.3	112.3	112.3	112.2
Annular argon, slpm	20	19.9	19.8	19.9
Total gas flow, slpm	187.8	188	188.1	187.8
Coating gas fraction	0.30	0.30	0.30	0.30
Coating gas ratio	0.85	0.84	0.84	0.86
Coating time, minutes	11.9	11.9	11.9	11.9
Coating rate, $\mu\text{m}/\text{min}$	3.29	3.47	3.81	3.60
IPyC thickness, $\mu\text{m}$	39.2	41.3	45.3	42.8
IPyC density, $\text{g}/\text{cm}^3$	1.898	1.893	Not measured	Not measured
IPyC BAF <sub>o</sub>	1.0387	1.0395	Not measured	Not measured
IPyC porosity, $\text{ml}/\text{m}^2$	2.2	2.2	Not measured	Not measured
<b>SiC</b>				
Control Temp, °C	1550	1600	1549	1600
Bed TC Temp, start, °C	NA	NA	NA	NA
Bed TC Temp, end, °C	NA	NA	NA	NA

Table A-6. (continued).

	Run ID			
	93059	93060	93061	93062
MTS flow, g/hr	1508	1210	1513	1018
H <sub>2</sub> flow, MTS sweep, slpm	40	40	41	40
H <sub>2</sub> flow, slpm	28.4	122.1	28.5	122
Annular H <sub>2</sub> flow, slpm	16.8	27	16.9	27
Argon, slpm	36.6	0	36.9	0
Total gas flow, slpm	121.8	189.1	123.3	189
Ar, mol %	30.0%	0	29.9%	0
Mole % MTS	3.02%	1.57%	2.97%	1.57%
Coating time, minutes	102	125	102	120
Coating rate, $\mu\text{m}/\text{min}$	0.34	0.29	0.31	0.23
SiC thickness, $\mu\text{m}$	34.3	36.8	31.9	27.5
SiC density, $\text{g}/\text{cm}^3$	3.199	3.195	3.195	3.193
SiC aspect ratio	1.039	1.036	1.033	1.038
SiC defects	5.2	10	2.7/4.7	0.8/0.8
SiC defect sample size	50,000	120,000	50,000x2	50,000x2
<b>OPyC</b>				
Control Temp, °C	1353	1352	1353	1352
Bed TC Temp, start, °C	NA	NA	NA	NA
Bed TC Temp, end, °C	NA	NA	NA	NA
Acetylene, slpm	36.7	36.6	36.8	36.8
Propylene, slpm	31.2	31	31.1	31.2
Argon, slpm	102.1	102.1	102.1	102.1
Annular argon, slpm	46	45.9	45.9	45
Total gas flow, slpm	216	215.6	215.9	215.1
Coating gas fraction	0.31	0.31	0.31	0.32
Coating gas ratio	0.85	0.85	0.85	0.85
Coating time, minutes	13.3	13.3	13.3	13.3
Coating rate, $\mu\text{m}/\text{min}$	2.95	2.93	3.22	3.20
OPyC thickness, $\mu\text{m}$	39.2	39	42.8	42.6
OPyC density, $\text{g}/\text{cm}^3$	1.914	1.911	1.912	1.893
OPyC BAF <sub>o</sub>	1.0282	1.0275	Not measured	Not measured
OPyC porosity, $\text{ml}/\text{m}^2$	0.5	0.7	0.6	0.6
OPyC aspect ratio	Not measured	Not measured	Not measured	Not measured
Missing OPyC	0/16,000	0/16,000	0/16,000	0/16,000
<b>Other/notes</b>				
SiC inclusions	0/6257	1/5917		

Table A-7. Coating parameter and particle properties for runs 93063-93066.

Run ID				
	93063	93064	93065	93066
<b>Kernels</b>				
Charge size, kg	1.3	1.3	1.3	1.3
Mean diameter, microns	432	432	432	421
Type	NUCO	NUCO	NUCO	NUCO
<b>Buffer</b>				
Control Temp, °C	1473	1473	1474	1474
Bed TC Temp, start, °C	NA	NA	NA	NA
Bed TC Temp, end, °C	NA	NA	NA	NA
Acetylene, slpm	97	97.5	97.5	97.5
Argon, slpm	39	39	39.1	39.1
Annular argon, slpm	26	26	26.1	26.1
Total gas flow, slpm	162	162.5	162.7	162.7
Coating gas fraction	0.60	0.60	0.60	0.60
Coating time, minutes	4.1	4.1	4.1	4.25
Coating rate, $\mu\text{m}/\text{min}$	23.07	24.39	23.68	23.88
Buffer thickness, $\mu\text{m}$	94.6	100	97.1	101.5
Buffer density, $\text{g}/\text{cm}^3$	Not measured	0.96	Not measured	0.96
<b>IPyC</b>				
Control Temp, °C	1328	1329	1329	1329
Bed TC Temp, start, °C	NA	NA	NA	NA
Bed TC Temp, end, °C	NA	NA	NA	NA
Acetylene, slpm	30	30	30	30
Propylene, slpm	25.5	25.7	25.7	25.6
Argon, slpm	112	112.3	112.3	112.3
Annular argon, slpm	19.9	19.8	19.8	19.8
Total gas flow, slpm	187.4	187.8	187.8	187.7
Coating gas fraction	0.30	0.30	0.30	0.30
Coating gas ratio	0.85	0.86	0.86	0.85
Coating time, minutes	10.51	10.51	10.51	12.3
Coating rate, $\mu\text{m}/\text{min}$	3.52	3.56	3.65	3.52
IPyC thickness, $\mu\text{m}$	37	37.4	38.4	43.3
IPyC density, $\text{g}/\text{cm}^3$	1.902	Not measured	1.884	Not measured
IPyC BAF <sub>o</sub>	1.0396	Not measured	Not measured	1.0336
IPyC porosity, $\text{ml}/\text{m}^2$	Not measured	Not measured	Not measured	Not measured
<b>SiC</b>				
Control Temp, °C	1600	1600	1549	1599
Bed TC Temp, start, °C	NA	NA	NA	NA
Bed TC Temp, end, °C	NA	NA	NA	NA

Table A-7. (continued).

	Run ID			
	93063	93064	93065	93066
MTS flow, g/hr	1400	1400	1432	1297
H <sub>2</sub> flow, MTS sweep, slpm	40	40	40	40
H <sub>2</sub> flow, slpm	122	121	28.4	121
Annular H <sub>2</sub> flow, slpm	27.1	27.1	16.8	27
Argon, slpm	0	0	36.9	0
Total gas flow, slpm	189.1	188.1	122.1	188
Ar, mol %	0	0	30.2%	0
Mole % MTS	1.81%	1.82%	2.85%	1.68%
Coating time, minutes	120	120	100	110.5
Coating rate, $\mu\text{m}/\text{min}$	0.33	0.33	0.35	0.32
SiC thickness, $\mu\text{m}$	39.8	39.3	34.5	35.4
SiC density, $\text{g}/\text{cm}^3$	3.194	3.191	3.197	3.193
SiC aspect ratio	1.032	1.036	1.033	1.032
SiC defects	<0.2	5.1	<0.2	4.3
SiC defect sample size	50,000	50,000	50,000	120,000
<b>OPyC</b>				
Control Temp, °C	1352	1352	1353	1353
Bed TC Temp, start, °C	NA	NA	NA	NA
Bed TC Temp, end, °C	NA	NA	NA	NA
Acetylene, slpm	36.4	36.6	36.5	36.6
Propylene, slpm	31.2	31.2	31.2	31.2
Argon, slpm	102	102.1	102.1	102.1
Annular argon, slpm	45.9	46	45.9	45.9
Total gas flow, slpm	215.5	215.9	215.7	215.8
Coating gas fraction	0.31	0.31	0.31	0.31
Coating gas ratio	0.86	0.85	0.85	0.85
Coating time, minutes	13.3	13.3	13.3	14
Coating rate, $\mu\text{m}/\text{min}$	3.11	3.08	2.86	3.04
OPyC thickness, $\mu\text{m}$	41.3	40.9	38	42.6
OPyC density, $\text{g}/\text{cm}^3$	1.904	1.903	1.906	1.896
OPyC BAF <sub>o</sub>	1.0257	Not measured	Not measured	1.0262
OPyC porosity, $\text{ml}/\text{m}^2$	0.8	0.8	0.4	0.6
OPyC aspect ratio	Not measured	Not measured	Not measured	Not measured
Missing OPyC	0/16,000	0/16,000	0/16,000	0/16,000
<b>Other/notes</b>				
	TC-7 replaced prior to run 93062			
OPyC porosity, $\text{ml}/\text{m}^2$ , hot sample	0.9		0.7	
SiC inclusions				0/5415

Table A-8. Coating parameter and particle properties for runs 93067-93070.

Run ID				
	93067	93068	93069	93070
<b>Kernels</b>				
Charge size, kg	1.3	1.3	1.3	1.3
Mean diameter, microns	421	421	421	426
Type	NUCO	NUCO	NUCO	LEU UCO
<b>Buffer</b>				
Control Temp, °C	1473	1474	1474	1474
Bed TC Temp, start, °C	NA	NA	NA	NA
Bed TC Temp, end, °C	NA	NA	NA	NA
Acetylene, slpm	97.1	97.4	97.3	96.4
Argon, slpm	39	39	39.1	39
Annular argon, slpm	26	26.1	26.1	25
Total gas flow, slpm	162.1	162.5	162.5	160.4
Coating gas fraction	0.60	0.60	0.60	0.60
Coating time, minutes	4.25	4.25	4.25	4.25
Coating rate, $\mu\text{m}/\text{min}$	23.41	21.79	22.99	22.96
Buffer thickness, $\mu\text{m}$	99.5	92.6	97.7	97.6
Buffer density, $\text{g}/\text{cm}^3$	Not measured	0.94	Not measured	Not measured
<b>IPyC</b>				
Control Temp, °C	1329	1329	1329	1329
Bed TC Temp, start, °C	NA	NA	NA	NA
Bed TC Temp, end, °C	NA	NA	NA	NA
Acetylene, slpm	30	30	30	30
Propylene, slpm	25.7	25.7	25.7	25.7
Argon, slpm	112.3	112.3	112.3	112.3
Annular argon, slpm	19.9	19.6	19.9	19.8
Total gas flow, slpm	187.9	187.6	187.9	188.0
Coating gas fraction	0.30	0.30	0.30	0.30
Coating gas ratio	0.86	0.86	0.86	0.86
Coating time, minutes	12.3	12.3	12.3	11.2
Coating rate, $\mu\text{m}/\text{min}$	3.50	3.59	3.61	3.63
IPyC thickness, $\mu\text{m}$	43.1	44.2	44.4	40.7
IPyC density, $\text{g}/\text{cm}^3$	1.889	Not measured	1.896	Not measured
IPyC BAF <sub>o</sub>	Not measured	Not measured	1.0335	Not measured
IPyC porosity, $\text{ml}/\text{m}^2$	2.1	Not measured	Not measured	Not measured
<b>SiC</b>				
Control Temp, °C	1598	1549	1549	1550
Bed TC Temp, start, °C	NA	NA	NA	NA
Bed TC Temp, end, °C	NA	NA	NA	NA

Table A-8. (continued).

	Run ID			
	93067	93068	93069	93070
MTS flow, g/hr	1280	1382	1430	1576
H <sub>2</sub> flow, MTS sweep, slpm	39	39.5	42	41
H <sub>2</sub> flow, slpm	122.5	29	26.4	26.2
Annular H <sub>2</sub> flow, slpm	27	16.9	16.8	16.5
Argon, slpm	0	36.8	36.9	36
Total gas flow, slpm	188.5	122.2	122.1	119.7
Ar, mol %	0	30.1%	30.2%	30.1%
Mole % MTS	1.67%	2.78%	2.81%	2.54%
Coating time, minutes	115	108.7	108	124
Coating rate, $\mu\text{m}/\text{min}$	0.31	0.33	0.34	0.30
SiC thickness, $\mu\text{m}$	35.7	36.1	36.8	36.9
SiC density, $\text{g}/\text{cm}^3$	3.196	3.204	3.204	Not measured
SiC aspect ratio	1.038	1.034	1.033	Not measured
SiC defects	0.5	<0.2	<0.1	Not measured
SiC defect sample size	50,000	50,000	50,000	
<b>OPyC</b>				
Control Temp, °C	1353	1353	1353	1353
Bed TC Temp, start, °C	NA	NA	NA	NA
Bed TC Temp, end, °C	NA	NA	NA	NA
Acetylene, slpm	36.6	36.5	36.4	35.5
Propylene, slpm	31.1	31.5	31.2	31.25
Argon, slpm	102.1	102.4	102.1	99.4
Annular argon, slpm	45.9	45.8	45.9	44.8
Total gas flow, slpm	215.7	216.2	215.6	210.9
Coating gas fraction	0.31	0.31	0.31	0.32
Coating gas ratio	0.85	0.86	0.86	0.88
Coating time, minutes	14	14	14	14
Coating rate, $\mu\text{m}/\text{min}$	2.94	2.76	2.21	3.02
OPyC thickness, $\mu\text{m}$	41.2	38.6	31	42.3
OPyC density, $\text{g}/\text{cm}^3$	1.897	1.901	1.898	Not measured
OPyC BAF <sub>o</sub>	Not measured	Not measured	1.0269	Not measured
OPyC porosity, $\text{ml}/\text{m}^2$	0.6	0.6	0.6	Not measured
OPyC aspect ratio	Not measured	Not measured	Not measured	Not measured
Missing OPyC	0/16,000	0/16,000	0/16,000	
<b>Other/notes</b>				
OPyC porosity, $\text{ml}/\text{m}^2$ , hot sample			0.9	
SiC defects, 2 <sup>nd</sup> sample of 70,000		<1.5	<0.1	



The DVD contains:

- Nozzle images following batches 93033 through 93073
- Particle images of batches 93033 through 93070
- Images of etched particles from batches 93035 through 93053
- SEM images from batches 93056 through 93069.

**PLEASE SEE THE NGNP RECORDS COORDINATOR  
AND/OR  
THE R&D FUEL FABRICATION WORK PACKAGE  
MANAGER FOR IMAGES OF APPENDIX A**

---